Surface biofunctionalization with liquid-phase plasma treatment of collagen molecules

Shiori Tanaka
Tokyo University of Agriculture and Technology
Shingo Kanemura
Kwansei Gakuin University
Masaki Okumura
Tohoku University
Kazuyuki Iwaikawa
Tokyo University of Agriculture and Technology
Kenichi Funamoto
Tohoku University https://orcid.org/0000-0002-0703-0910
Godai Miyaji
Tokyo University of Agriculture and Technology
Takahiro Muraoka
Tokyo University of Agriculture and Technology https://orcid.org/0000-0001-6744-048X
Kazuhiko Misawa
Tokyo University of Agriculture and Technology (TUAT) https://orcid.org/0000-0002-7150-2097
Daisuke Yoshino (uirooo@gmail.com)
Tokyo University of Agriculture and Technology https://orcid.org/0000-0002-2948-1210

Article

Keywords: substrate biofunctionalization, collagen, liquid-phase plasma discharge

Posted Date: August 20th, 2021

DOI: https://doi.org/10.21203/rs.3.rs-677830/v2

Title: Surface biofunctionalization with liquid-phase plasma treatment of collagen molecules

Authors:

Shiori Tanaka[1,2], Shingo Kanemura[3], Masaki Okumura[4], Kazuyuki Iwaikawa[1], Kenichi Funamoto[5], Godai Miyaji[1,6,7], Takahiro Muraoka[1,6,8], Kazuhiko Misawa[1,6,7], Daisuke Yoshino[1,6,7]*

Affiliations:

[1] School of Engineering, Tokyo University of Agriculture and Technology, 2-24-16 Naka-cho, Koganei, Tokyo 184-8588, Japan

[2] Graduate School of Bio-Applications and Systems Engineering, Tokyo University of Agriculture and Technology, 2-24-16 Naka-cho, Koganei, Tokyo 184-8588, Japan

[3] School of Science, Kwansei Gakuin University, 2-1 Gakuen, Sanda, Hyogo 669-1337, Japan

[4] Frontier Research Institute for Interdisciplinary Sciences, Tohoku University, 6-3 Aramaki-Aoba, Aoba-ku, Sendai 980-8578, Japan

[5] Institute of Fluid Science, Tohoku University, 2-1-1 Katahira, Aoba-ku, Sendai 980-8577, Japan

[6] Graduate School of Engineering, Tokyo University of Agriculture and Technology, 2-24-16 Naka-cho, Koganei, Tokyo 184-8588, Japan

[7] Institute of Engineering, Tokyo University of Agriculture and Technology, 2-24-16 Naka-cho, Koganei, Tokyo 184-8588, Japan

[8] Institute of Global Innovation Research, Tokyo University of Agriculture and Technology, 2-24-16 Naka-cho, Koganei, Tokyo 184-8588, Japan

***Corresponding author:**

dyoshino@go.tuat.ac.jp (Daisuke Yoshino, Ph.D.)

Abstract

Surface functionalization is a key process in rendering various materials biocompatible. Whereas a number of techniques and technologies have been developed for the purpose of biofunctionalization, plasma treatment enables highly efficient surface modification. Extending plasma treatment to biomolecules in the liquid phase will control biofunctionalization via a simple process. However, interactions between plasma discharge and biomolecules or solvents are poorly understood, potentially leading to the technical limitation as to the utility of plasma treatment. In this study, we developed a technology for substrate biofunctionalization that does not require surface modification but involves direct treatment of a collagen molecules with liquid-phase plasma discharge. Biofunctionalization of collagen by plasma treatment comprises three processes that increase its reactivity with hydrophobic substrates: (1) charge-dependent changes in surface and interfacial properties of the collagen solution; (2) local conformational changes of the collagen molecules without their global structural alterations; and (3) induction of a micelle-like association formed by collagen molecules. We anticipate such plasma-induced functionalization of protein molecules to provide a versatile technique in the applications of biomaterials, including those related to pharmaceuticals and cosmetics.

Main text:

Introduction

Biofunctionalization is important for treating disease and improving prognosis by increase in the biocompatibility of implantable medical devices. Chemical modification of biomolecules [1, 2] and surface modification with nonthermal plasma [3] are often used for biofunctionalization of medical devices. Surface modification with nonthermal plasma in particular enhance cell adhesiveness and the hydrophilicity of the medical devices such as catheters, stents, and artificial bones and organs, which are typically constructed of heat-sensitive materials, by a simple process [4-6]. Although plasma surface modification seems to offer unlimited applications, there are some drawbacks. For example, plasma modification results in uneven treatment of objects with fine and complex shapes. Micro-spotting of the plasma source to overcome this problem makes the process more complicated. Plasma modification is also not applicable to objects covered with highly reactive materials or solutions because the plasma will react with such materials and solutions before the flow reaches the target surface. Taking advantage of these drawbacks, we hypothesized that functionalization of biomolecules in solution using direct plasma treatment could uniformly enhance the cell adhesiveness of targets with fine and complex shapes. A detailed understanding of the mechanisms through which plasma interacts with biomolecules and solvent molecules will be necessary to validate our hypothesis (*i.e.*, establishment of a biofunctionalization technology is possible). The interaction between plasma and solution molecules has been clarified in terms of the transfer of charged particles into the solution [7-9], the generation of reactive chemical species and ions [8, 10], and oxidation-reduction reactions [11, 12]. These effects of plasma discharge can be used to synthesize nanoparticles composed of polymers and metals [13-16]. However, our understanding of how plasma interacts with biomolecules in solution, including proteins, remains limited.

In this study, we developed a technology for the biofunctionalization of target substrates without surface modification via direct treatment of a solution of collagen (an extracellular matrix [ECM] protein) with liquid-phase plasma discharge. We found that plasma treatment induced charge-dependent changes in the surface and interfacial properties of the collagen solution. We also found that plasma treatment altered the local conformation of the collagen molecules without affecting their global structure, inducing

them to assume a micelle-like association. These plasma-induced changes play key roles in substrate biofunctionalization.

Results

Liquid-phase surface discharge plasma.

We first established generation of surface discharge plasma in a liquid phase (**Fig. 1a-c**; patent no. JP6713795B), which has been considered impossible. This plasma source allows for relatively weak treatment of biomolecules in solution. Here, we examined the characteristics of the liquid-phase surface discharge plasma source. In the absence of a solution, plasma emission was observed at the tip of the applied electrode on the inner surface of the glass tube (**Fig. 1b**), and its spectra exhibited peaks at 315.9, 337.1, 357.7, 375.5, and 380.5 nm (**Fig. 1d**). These emission peaks, which are commonly found in atmospheric pressure plasma discharges, were attributed to the second positive system of nitrogen (N_2-SPS) [17]. The emission characteristics of this plasma source exhibited a similar trend, with some attenuation observed when ultrapure water, acetic acid solution, or collagen solution was in-flowed into the glass tube electrode (**Fig. 1e** and **f**, and **Supplementary Fig. 1**). Various chemical reactions occurred at the gas-liquid interface during plasma discharge, which resulted in the formation of oxidative products in the solution [8]. Our plasma source also produced oxidative compounds such as hydrogen peroxide (**Fig. 1g**), nitrite ion (**Fig. 1h**), and nitrate ion (**Fig. 1i**) in each solution. The concentrations of the oxidative compounds that were produced were generally low, ranging as high as 1.5 mg/L, although the concentrations varied slightly depending on solution type. Plasma treatment did not change the pH of the acetic acid or collagen solutions, which were buffered by acetic acid, but the pH of ultrapure water decreased from 6.3 to 5.0 upon plasma treatment (**Fig. 1j**).

Biofunctionalization of hydrophobic substrates with plasma-treated collagen.

We then evaluated the biofunctionalization of silicone-coated hydrophobic cover glass with collagen solution treated using the characterized plasma source. Human umbilical vein endothelial cells (HUVECs) adhered and spread on the hydrophobic cover glass during a 24-h incubation (P-Coll; **Fig. 2a**). In comparison with untreated collagen solution, acetic

acid solution, and ultrapure water, the plasma-treated collagen coating encouraged the adhesion of significantly more HUVECs and the formation of an endothelial monolayer (**Fig. 2a** and **b**). The plasma-treated collagen coating also stabilized the attachment of vinculin (a focal adhesion–associated adaptor protein [18]) to each cell (**Fig. 2c-e**). The biofunctionalization-enhancing effects of plasma-treated collagen were independent of the coating processing time (**Supplementary Fig. 2**). In the proliferation assay, HUVECs exhibited stable growth and formed a confluent monolayer without intercellular gaps on the hydrophobic cover glass coated with plasma-treated collagen (**Fig. 2f** and **g**). Vinculin attachment differed significantly between the plasma-treated collagen coating and the other conditions (**Fig. 2h-j**), possibly because HUVECs are known to produce ECM proteins, including collagen [19, 20]. These data thus demonstrate that plasma-treated collagen coating enhances the biofunctionalization of hydrophobic substrates.

Plasma-induced enhancement of the quality of collagen coating is a key factor in biofunctionalization.

We then investigated the cause of biofunctionalization (*i.e.*, why HUVECs adhere to and proliferate better on hydrophobic cover glass coated with plasma-treated collagen solution). Plasma-treated collagen was distributed uniformly on the hydrophobic cover glass, whereas untreated collagen was distributed locally, and voids were apparent (**Fig. 3a**). We hypothesized that the quality of the collagen coating affects the adhesion and proliferation of HUVECs on the cover glass. This hypothesis is supported by quantitative analysis of the data, which revealed a high average fluorescence intensity (**Fig. 3b**) and low degree of variation in the plasma-treated collagen solution in the coated state (**Fig. 3c**). Focusing on the wettability of the plasma-treated collagen solution, we therefore examined the surface and interfacial properties, which are related to the solution's surface tension and contact angle, respectively. Plasma treatment induced a time-dependent decrease in the contact angle of the collagen solution on the hydrophobic cover glass (**Fig. 3d** and **e**). In ultrapure water or acetic acid solution, the contact angle transiently decreased (up to 90 s after drop adhesion) and then recovered to near the initial value (**Supplementary Fig. 3**). Plasma treatment also produced a sustained decrease in the surface tension of the collagen solution (**Fig. 3f**) and a transient decrease in the surface tension of other solutions (**Supplementary Fig. 4**). The effect of evaporation on the results of contact angle analyses cannot be neglected due to the small volume of a droplet (1.5 μL) [21]. Indeed, a time

course analysis of droplet size showed a clear decrease in volume (**Supplementary Movie 1**). However, surface tension measured using the capillary rise method, which is not affected by evaporation, exhibited a similar time-dependent decrease in plasma-treated collagen solution (**Fig. 3f**). We thus conclude that plasma treatment induces time-dependent variations in the surface and interfacial properties of collagen solution (*i.e.*, an increase in the wettability of the collagen solution and consequent enhancement of coating quality).

Electric charge regulates the surface and interfacial properties of the solution.

To examine the cause of the observed plasma-induced changes in the surface and interfacial properties of collagen solution, we considered the possibility that the hydrophobic surface of the cover glass undergoes modification by chemical species in the solution [22-24]. However, we could not confirm changes in the contact angle of collagen solutions containing hydrogen peroxide, nitrite ion, or nitrate ion similar to those observed in plasma-treated collagen solution (**Fig. 4a** and **b** and **Supplementary Fig. 5**). Similarly, no reduction in surface tension was observed following addition of these chemical species to the collagen solution (**Fig. 4c** and **Supplementary Fig. 6**). Even in ultrapure water, chemical species had no effect on the surface and interfacial properties (**Supplementary Fig. 7**). Hence, chemical species at concentrations generated in solution by plasma treatment (**Fig. 1h-j**) do not markedly affect the surface and interfacial properties, nor do the chemical species modify the surface of the hydrophobic cover glass.

We then investigated the effect of electric charge on surface and interfacial properties. Several previous studies have examined the effects of electric fields on contact angle and surface tension [25-27]. Using a polystyrene dish covered with a grounded aluminum sheet, we released the electric charge supplied to the collagen solution by plasma treatment. Release of the electric charge from the collagen solution eliminated plasma-induced time-dependent decreases in the solution's contact angle (**Fig. 4d** and **e**) and surface tension (**Fig. 4f**).

Our results suggest that electric charge is the primary factor mediating plasma-induced changes in surface and interfacial solution properties, leading to an increase in the wettability of the collagen solution. This scenario is supported by findings demonstrating that plasma-treated collagen solution in which the electric charge was released lost its

effectiveness in promoting cell adhesion (**Fig. 4g** and **h**) and proliferation (**Fig. 4l** and **m**) when coated on the hydrophobic substrate. The loss of the coating effect of plasma-treated collagen also affected the attachment of vinculin to HUVECs in the cell adhesion assay (**Fig. 4i-k**). However, loss of the coating effect did not decrease endothelial attachment of vinculin in the cell proliferation assay (**Fig. 4n-p**), and one possible reason for this is self-production of ECM proteins by the HUVECs [19, 20].

Plasma changes the local conformation and association of collagen molecules, which play crucial roles in biofunctionalization.

Even the collagen solution in which the charge was released after plasma treatment enhanced the biofunctionalization of the hydrophobic substrate to some extent upon coating for an extended period (**Fig. 5a-e**). We therefore hypothesized that plasma treatment induces changes in collagen molecules themselves which contribute to biofunctionalization, in addition to the changes induced in the surface and interfacial properties of the solution. We confirmed that the collagen molecules were thermally denatured by plasma treatment. In electrophoresis, we observed clear bands similar to those of untreated collagen, as opposed to the unclear band pattern of gelatinized collagen that was boiled for 1 h (**Fig. 5f**). Hence, plasma treatment did not induce any noticeable change in the molecular weight of collagen or in the abundance ratios of its secondary structures. In addition, plasma treatment did not denature small structures such as epitopes involved in antigen-antibody reactions (**Fig. 5g**).

To further examine the effects of plasma treatment on collagen molecules, we analyzed their structure in more detail. Circular dichroism spectra of collagen were similar regardless of the treatment condition (**Fig. 5h**). We confirmed that there were no significant changes in the secondary structure of collagen molecules specifically caused by plasma treatment. Focusing on the primary structure of collagen molecules, we then found that plasma treatment reduced the total amount of hydroxyproline, one of the amino acids [28] of which collagen is composed (**Fig. 5i**). This decrease in hydroxyproline content was not attributed specifically to plasma treatment but rather to the chemical species produced in the solution (**Fig. 5j**). These results led to the conclusion that the slight structural changes in collagen molecules due to chemical species do not directly contribute to biofunctionalization of the hydrophobic substrate.

In contrast, plasma treatment induced a slight increase in the viscosity of the collagen solution (**Supplementary Fig. 8**). We thus investigated the association and bonding states of the collagen molecules to elucidate the core mechanism of plasma treatment. Raman spectra of collagen solution after plasma treatment exhibited peaks specific to collagen (**Fig. 6a** and **Supplementary Fig. 9**). Two of these peaks were not derived from the chemical species produced by plasma treatment, and they remained in spectra of collagen solution in which the charge was released after plasma treatment (**Fig. 6a** and **b** and **Supplementary Fig. 9**). These two peaks are related to the local conformation around hydroxyproline (876 cm^{-1}) and proline (1445 cm^{-1}; this peak indicates the absence of hydrogen bonding in X-PRO carbonyl groups) [29-32]. Hydroxyproline and proline play crucial roles in determining collagen stability [33] and permit the sharp twisting of the collagen triple helix [34]. Plasma treatment, therefore, induces changes in the local conformation, including hydrogen bonding states, of these amino acid side chains, which loosens the collagen helix.

We also measured the particle size of collagen associations based on dynamic light-scattering analysis (**Fig. 6c** and **d**). A comparison of peak values of collagen associations revealed that plasma treatment caused an increase in particle size (**Fig. 6e**). This was also true for the charge-released collagen solution, and the effect was not associated with chemical species (**Fig. 6f**). These results suggest that collagen molecules form micelle-like associations upon plasma treatment. This hypothesis is supported by our findings demonstrating that plasma treatment increased the fluorescence intensity of 8-anilino-1-naphthalenesulfonic acid (ANS) [35] in the collagen solution (**Fig. 6g**), indicating that plasma treatment alters the positions of hydrophobic sites. This alteration was also observed when the charge in the solution was released (**Fig. 6h**) but was not observed in a solution with added chemical species (**Fig. 6i**).

Based on these results, we conclude that plasma-induced changes in the local conformation and association of collagen molecules also play key roles in the biofunctionalization of hydrophobic surfaces. These findings can be explained by the fact that the surface and interfacial properties of a collagen solution differ from those of ultrapure water or acetic acid after plasma treatment (**Fig. 3e** and **f** and **Supplementary Figs. 3** and **4**).

Discussion

In this study, we developed a technology for the biofunctionalization of hydrophobic substrates using plasma-activated collagen. This biofunctionalization is driven by three processes that increase the reactivity of collagen molecules with hydrophobic substrates (**Supplementary Fig. 10**): (1) plasma charges the collagen solution and then causes alterations in the surface and interfacial properties of the solution, leading to an increase in wettability on the hydrophobic surface; (2) plasma treatment changes the local conformation of collagen molecules, including hydrogen bonding states, but does not induce any significant changes in their global structure; and (3) interaction of collagen molecules with plasma leads to forming their micelle-like associations. By better understanding the plasma-induced functionalization of other biomolecules as well, a variety of applications for plasma treatment could emerge, such as in pharmaceuticals and cosmetics, not to mention the biofunctionalization of target substrates.

The plasma-induced changes in collagen, which are the key to biofunctionalization of hydrophobic substrates in this study, are due to the fact that relatively weak treatment of collagen is made possible by surface discharge plasma in the liquid phase. Plasma-induced mechanochemical or electrochemical effects lead to the polymerization of molecules [36-38] and the synthesis of nanoparticles of polymers or metals [13-16]. Such plasma polymerization and synthesis procedures are usually carried out in the gas phase or at the gas-liquid interface. Gas-liquid interfacial plasma generates OH radicals and other reactive species in solution, which can affect the polymerization of polymers in solution. Our plasma source was discharged primarily in the liquid phase, with intermittent switching between the gas and liquid phases, and did not induce polymerization, (*i.e.*, gelation) of the collagen in solution. There was no noticeable change in the molecular weight of collagen as a result of the plasma-induced oxidation-reduction reaction. Plasma-induced changes in the local conformation and association of the collagen molecules, as demonstrated in the present study, differ from the commonly known changes associated with plasma polymerization and synthesis.

The mechanisms elucidated in the present study are based on indirect measurements and considerations, particularly in regard to the local conformation and association states of collagen molecules. We have not been able to directly determine how plasma treatment changes the local conformation of collagen molecules, loosens the collagen helix, or induces the micelle-like association of collagen molecules. This limitation is attributed to the time-dependent nature of plasma-induced changes in the collagen

276 solution and collagen molecules, which makes it technically difficult to perform assays that
277 are typically time consuming, such as structural analyses. The solution in-flow rate was
278 fixed at 1 mL/min in view of the temperature increase caused by plasma treatment. By
279 slowing the in-flow rate while controlling the temperature, it becomes possible to increase
280 the efficiency of collagen functionalization, as revealed in this study. We believe that
281 consideration of the treatment conditions will enable us to sustain the plasma-induced
282 functionalization of collagen and fully elucidate the underlying mechanisms.

Methods

Collagen solution. Collagen, a common ECM protein, was used for target biofunctionalization. A solution of collagen I, rat tail (A10483-01, Gibco, Thermo Fisher Scientific, Waltham, MA, USA and 08-115, Merck, Darmstadt, Germany) was prepared at 50–1000 μg/mL by dissolving in 20 mM acetic acid (017-00256, Wako Pure Chemical Industries, Osaka Japan). For comparison, we also treated ultrapure water and 20 mM acetic acid with surface discharge plasma.

Surface discharge plasma and its characterization. Surface discharge plasma was generated in a borosilicate glass tube with outer and inner diameters of 8 mm and 6 mm, respectively (**Fig. 1a** and **b**). The pulse voltage was applied to an aluminum sheet electrode attached onto the inner surface of the tube. An aluminum electrode attached on the outside across the glass was grounded. The applied voltage was +8 kV from 0 to peak, with a frequency of 5 kHz (**Fig. 1c**), which was confirmed using a high-voltage probe (P6015A, Tektronix, Beaverton, OR, USA).

Light emission from the charged plasma was recorded with a digital camera (X-T4, Fujifilm, Tokyo, Japan) equipped with a macro lens (XF80mmF2.8 R LM OIS WR Macro, Fujifilm). Emission spectra were measured using a high-resolution spectrometer (HR4000CG-UV-NIR, Ocean Insight, Orlando, FL, USA).

Surface discharge plasma treatment. The prepared solution was in-flowed through a fluorocarbon polymer tube into the glass tube electrode using a syringe pump (Legato 110, KD Scientific, Holliston, MA, USA). The in-flowed solution was then treated with surface discharge plasma. The in-flow rate of the solution was 1 mL/min. Treated solution was collected in a polystyrene dish (3000-035, AGC Techno Glass, Shizuoka, Japan). To exclude any effects of electric charge, we also collected the solution in a polystyrene dish covered with a grounded aluminum sheet.

Chemical species detection. The production of hydrogen peroxide, nitrite ion, and nitrate ion was examined because these species are reportedly generated by plasma-liquid interactions [8]. Hydrogen peroxide, nitrite ions, and nitrate ions present in the solutions (ultrapure water, 20 mM acetic acid solution, and 50 μg/mL collagen solution) were detected using 4-aminoantipyrine colorimetric assay (WAK-H2O2, Kyoritsu Chemical-Check Lab, Tokyo, Japan), naphthyl ethylenediamine colorimetric assay (WAK-NO2, WAK-NO3, Kyoritsu Chemical-Check Lab), and Griess assay (NK05, Dojindo Laboratories,

315 Kumamoto, Japan) kits, respectively. The absorbance was monitored in each assay using
316 an absorptiometer (DPM-MTSP, Kyoritsu Chemical-Check Lab or iMark, Bio-Rad
317 Laboratories, Hercules, CA, USA). The concentration of each chemical species was then
318 determined based on the measured absorbance and a calibration curve. The pH of each
319 solution was measured using a pH meter (LAQUAtwin; AS-pH-11B, AS ONE, Osaka,
320 Japan).

321 **Substrate preparation.** A silicone-coated hydrophobic cover glass (C2240, Matsunami
322 Glass Industry, Osaka, Japan) was biofunctionalized with plasma-treated collagen solution.
323 The hydrophobic cover glass was immersed in the plasma-treated collagen solution (50
324 μg/mL) for 3 min and then allowed to completely air dry. For comparison, a cover glass was
325 also immersed in untreated collagen solution, 20 mM acetic acid, or ultrapure water for 3
326 min. To evaluate the effect of treatment time on biofunctionalization, we also examined
327 hydrophobic cover glass samples immersed in plasma-treated or untreated collagen
328 solution for 1 h.

329 **Antibodies.** Mouse monoclonal anti-vinculin antibody (26520-1-AP, dilution; 1:500
330 [Immuno-fluorescence; IF]) was purchased from Proteintech (Rosemont, IL, USA). Mouse
331 monoclonal anti-VE-cadherin antibody (sc-9989, dilution; 1:100 [IF]) and mouse monoclonal
332 anti-COL1A antibody (sc-59772, dilution; 1:100 [IF] and 1:1000 [Western blotting; WB])
333 were purchased from Santa Cruz Biotechnology (Dallas, TX, USA). Alexa Fluor 488–
334 conjugated goat anti-mouse IgG (A28175, dilution; 1:200 [IF]), Alexa Fluor 594–conjugated
335 goat anti-mouse IgG (A11032, dilution; 1:200 [IF]), and Alexa Fluor 488–conjugated goat
336 anti-rabbit IgG (A27034, dilution; 1:200 [IF]) secondary antibodies were purchased from
337 Thermo Fisher Scientific. Horseradish peroxidase–conjugated anti-mouse IgG (7076S,
338 dilution; 1:5000 [WB]) was purchased from Cell Signaling Technology (Danvers, MA, USA).

339 **Cell culture.** HUVECs (200-05n, Cell Applications, San Diego, CA, USA) were cultured in
340 Medium 199 (31100-035, Gibco, Thermo Fisher Scientific) containing 20% heat-inactivated
341 fetal bovine serum (12483-020, Gibco), 10 μg/L human basic fibroblast growth factor (GF-
342 030-3, Austral Biologicals, San Ramon, CA, USA), and 1% penicillin/streptomycin (15140-
343 122, Gibco). HUVECs from the fifth to ninth passages were used for experiments in this
344 study.

345 **Cell adhesion assay.** HUVECs were seeded on the prepared glass substrate at a density
346 of 4×10^4 cells/cm^2. The cells were then incubated with culture medium in a CO_2 incubator.

After 24 h of incubation, adherent HUVECs were observed using a phase-contrast microscope (CKX41, Olympus, Tokyo, Japan) equipped with a sCMOS camera (WRAYCAM-SR 130 M, WRAYMER, Osaka, Japan). Based on the captured images, the number of cells per unit area was determined using ImageJ Fiji software (US National Institutes of Health) [39].

Cell proliferation assay. HUVECs were seeded on the prepared glass substrate at a density of 1×10^4 cells/cm^2. The cells were then incubated with culture medium in a CO_2 incubator for up to 72 h, with replacement of the medium every day. Images of HUVEC proliferation were captured using a phase-contrast microscope every 24 h after cell seeding. The number of cells per unit area was then determined based on the captured images.

Immunofluorescence staining. After cell adhesion and proliferation assays, HUVECs were fixed with 4% paraformaldehyde phosphate buffer solution (163-20145, Fujifilm Wako Pure Chemical Corporation, Osaka, Japan). The cells were permeabilized with 0.1% TritonX-100 (17-1315-01, Pharmacia Biotech, Uppsala, Sweden) in phosphate-buffered saline (PBS; 05913, Nissui Pharmaceutical, Tokyo, Japan) and incubated in 1% Block Ace (BA; UKB40, DS Pharma Biomedical, Osaka, Japan) to prevent nonspecific antibody adsorption. The cells were then stained using primary and secondary antibodies diluted in 1% BA in PBS and PBS, respectively, at predefined concentrations. Cell nuclei and actin filaments were stained using 4',6-diamidino-2-phenylindole (D1306, Thermo Fisher Scientific) and Alexa Fluor 488–conjugated phalloidin (A12379, Thermo Fisher Scientific), respectively. Stained HUVECs were observed using a wide-field fluorescence microscope (BX51WI, Olympus). For staining of collagen coated onto the hydrophobic cover glass, the blocking process and subsequent steps described above were performed.

Vinculin attachment points. Adhesion of cells to the biofunctionalized glass substrate was evaluated based on the number of attachment points of a focal adhesion–associated adaptor protein, vinculin. We first prepared a fluorescence image minus background noise based on the fluorescence intensity threshold using the function “subtract background-rolling” in ImageJ Fiji. The number of vinculin particles was then counted as vinculin attachment points from the binarized images using the function “analyze particles”. The number of cells was determined based on counting of fluorescent-stained cell nuclei and calculated vinculin attachment points per cell.

Fluorescence intensity of COL1A. Fluorescence images of six arbitrary locations were captured for each hydrophobic cover glass. Fluorescence intensity and standard deviation of stained COL1A were determined for a rectangular region of 3,000 × 3,000 pixels (240 × 240 μm) using ImageJ Fiji.

Contact angle analysis. To evaluate the wettability of the plasma-treated solutions (ultrapure water, 20 mM acetic acid solution, and 50 μg/mL collagen solution), the contact angle was measured on the silicone-coated hydrophobic cover glasses using a contact angle meter (Smart Contact Mobile 4, Excimer Inc., Yokohama, Japan). Images of 1.5-μL solution droplets were captured every 10 s from 150 s to 300 s after the start of surface discharge plasma treatment. The contact angle was calculated based on the θ-2θ method using ImageJ Fiji.

Surface tension measurement. Surface tension of the solution was measured based on the capillary rise method [40] using a borosilicate glass capillary (9600150, Ringcaps® Disposable Capillary Pipettes 1 Mark 50 μL, Hirschmann Laborgeräte GmbH & Co., Eberstadt, Germany) with inner diameter of 1.05 mm. Capillary action (*i.e.* rise of the solution [ultrapure water, 20 mM acetic acid solution, or 50 μg/mL collagen solution]) at 150, 240, and 300 s after the start of plasma treatment was photographed using a digital camera and macro lens. The contact angle of the solution at the capillary inner wall and the height of the solution level were measured using ImageJ Fiji. The surface tension, γ, was obtained from the following equation:

$$\gamma = r\rho g / 2\cos\theta,$$

where r, ρ, g, and θ represent the inner radius of the glass capillary, the solution density, the gravitational acceleration, and the contact angle of the solution, respectively.

Electrophoresis and immunoblotting. Collagen molecules were collected from the plasma-treated solution (50 μg/mL collagen solution) according to the following protocol. Acetic acid buffer (20 mM) was removed from the plasma-treated collagen solutions (480 μL each) after washing twice with ultrapure water and centrifugation (20,000*g* at 4ºC for 10 min) using an ultrafiltration spin column (PT-1002, Integrale, Tokyo, Japan). The extracted collagen molecules were resuspended in Laemmli sample buffer (161-0747, Bio-Rad Laboratories) containing 20 mM dithiothreitol (161-0611, Bio-Rad Laboratories). Samples (12 μg collagen each) were subjected to SDS-PAGE using a Criterion TGX gel (gel concentration: 10%; 567-1034J10, Bio-Rad Laboratories). The gel was stained with

Coomassie Brilliant Blue (161-0436, Bio-Rad Laboratories) and then scanned with ChemiDoc XRS+ (Bio-Rad Laboratories).

After SDS-PAGE, samples were also transferred onto an Immun-Blot PVDF membrane (162-0177, Bio-Rad Laboratories). The membrane was blocked with Tris-buffered saline containing 1% BA and 0.05% Tween 20 and then stained using primary and secondary antibodies diluted in Can Get Signal Immunoreaction Enhancer Solution (NKB-101, Toyobo, Osaka, Japan). The blotted collagen bands were detected and visualized using Clarity Western ECL Substrate (170-5061, Bio-Rad Laboratories). The molecular weight of each sample was determined based on Precision Plus Protein Dual Color Standards (161-0374, Bio-Rad Laboratories).

Collagen solutions not treated with plasma and collagen solution boiled for 1 h were also analyzed for comparison.

Viscosity measurement. Viscosity of the plasma-treated collagen solution (50 μg/mL) was analyzed using a viscometer (VM-10A, SEKONIC, Tokyo, Japan). The volume of solution required for the measurement was approximately 5 mL. The temperature change of the solution during measurement was adjusted to ±0.5ºC. The temperature of the solution was measured using a digital thermometer (CT-320WP, Custom, Tokyo, Japan).

Circular dichroism spectroscopy. Circular dichroism spectra were collected to visualize the secondary structure of collagen molecules. Plasma-treated collagen solution (50 μg/mL) was placed into a quartz glass cell (S15-UV-2, GL Sciences, Tokyo, Japan), and the spectra were collected using a circular dichroism spectrometer (J-1100, JASCO Corporation, Tokyo, Japan). Spectra of the solvent (20 mM acetic acid solution) were subtracted from the results as background.

Hydroxyproline assay. Samples were prepared by acid hydrolysis of collagen by adding hydrochloric acid to plasma-treated collagen solution (1 mg/mL) to a final concentration of 4 M, followed by boiling for 1 h. The amount of hydroxyproline inside the collagen molecules was determined using a hydroxyproline assay kit (QZBhypro1, QuickZyme Biosciences, Leiden, Netherlands) according to the manufacturer's instructions.

Raman spectroscopy. Raman spectra of plasma-treated collagen solution (50 μg/mL) were collected using a spontaneous Raman spectroscopy system consisting of an EM-CCD camera, a single-mode laser (wavelength = 532 nm), and spectrometer (center wavelength

= 570 nm) [41, 42]. After plasma treatment, the solution was placed in a quartz glass cuvette (1 × 10 mm in dimensions) for analysis (S15-UV-1, GL Sciences, Tokyo, Japan), and Raman spectra were obtained at the center of the optical path. Each exposure time was set to 3 min, and the spectra were calculated from the accumulation of 10 measurements.

Particle size analysis. The size distribution of collagen associations was measured based on dynamic light scattering using a Zetasizer Nano (ZSP, Malvern Panalytical Ltd., Malvern, UK). Two milliliters of plasma-treated collagen solution was transferred to a polystyrene cuvette (67.754, Sarstedt, Nümbrecht, Germany) for measurement immediately after treatment, and the measurement chamber was kept at 25°C. Each exposure time was set to 10 s, and the size distribution was calculated from 11 accumulated measurements. Four measurements were obtained for each of three samples. Peak values were evaluated by excluding particles >100 nm in size (**Fig. 6c** and **e**), which were considered debris originating from electrode erosion caused by the plasma discharge [43, 44]. In the experiment examining the effect of chemical species, no debris was observed because the samples were prepared without using the discharge apparatus (**Fig. 6d** and **f**).

ANS binding assay. Conformational changes in collagen molecules were evaluated based on the fluorescence intensity of ANS (A0472, Tokyo Chemical Industry Corporation, Tokyo, Japan). The fluorescent properties of ANS change as the molecule reacts with hydrophobic regions on the protein surface [35]. Comparisons of fluorescence intensities can thus give information about the transition between the hydrophilic and hydrophobic states of collagen molecules triggered by plasma treatment. ANS was added to 50 μg/mL collagen solution to achieve a final concentration of 1 mM. The fluorescence intensity of ANS in each solution was measured with excitation at 370 nm and emission at 400–600 nm using a multi-grating microplate reader (SH-9000Lab, Corona Electric Corporation, Ibaraki, Japan).

Statistics and reproducibility. All values are shown as mean ± standard deviation (SD) unless stated otherwise. All data were obtained from at least three independently repeated experiments. Statistical significance was evaluated using the two-sided Welch's *t* test with Bonferroni correction for multiple comparisons, with statistical significance set at $p \leq 0.05$.

Data availability

The authors declare that all data supporting the findings of this study are available within this article and its supplementary information files or from the corresponding author upon reasonable request.

Conflicts of interest

Patents associated with the surface discharge plasma source and technique for biofunctionalization using the source have been registered in Japan (JP6408689B, JP6713795B).

Acknowledgements

The authors thank Prof. M. Ukai of Tokyo University of Agriculture and Technology for his expert advice on plasma emission spectroscopy. The Japan Society for the Promotion of Science (JSPS KAKENHI grant number 18K19894) and Japan Science and Technology Agency (Building of Consortia for the Development of Human Resources in Science and Technology) are acknowledged for financial support.

Author contributions

D.Y. conceived and designed the research. S.T. conducted most of the experiments. S.K. and M.O. conducted ANS binding assays. K.I. and K.M. were responsible for Raman spectroscopy. K.F. conducted viscosity measurements. G.M. provided support for plasma spectrometric analyses. T.M. provided technical assistance for circular dichroism spectroscopy and particle size analyses. All authors discussed the data. S.T. and D.Y. wrote the manuscript. D.Y. directed and supervised the project.

References

1. Yuan, L., Yu, Q., Li, D. & Chen, H. Surface modification to control protein/surface interactions. *Macromol. Biosci.* **11**, 1031-1040, https://doi.org/10.1002/mabi.201000464 (2011).
2. Sun, W., Liu, W., Wu, Z. & Chen, H. Chemical surface modification of polymeric biomaterials for biomedical applications. *Macromol. Biosci.* **41**, 1900430, https://doi.org/10.1002/marc.201900430 (2020).
3. Jacobs, T. et al. Plasma surface modification of biomedical polymers: Influence on cell-material interaction. *Plasma Chem. Plasma Process.* **32**, 1039-1073, https://doi.org/10.1007/s11090-012-9394-8 (2012).
4. Morent, R., De Geyter, N., Desmet, T., Dubruel, P. & Leys, C. Plasma surface modification of biodegradable polymers: A review. *Plasma Process. Polym.* **8**, 171-190, https://doi.org/10.1002/ppap.201000153 (2011).
5. Jelil, R. A. A review of low-temperature plasma treatment of textile materials. *J. Mater. Sci.* **50**, 5913-5943, https://doi.org/10.1007/s10853-015-9152-4 (2015).
6. Shim, J. W. et al. Hydrophilic surface modification of coronary stent using an atmospheric pressure plasma jet for endothelialization. *J. Biomater. Appl.* **32**, 1083-1089, https://doi.org/10.1177/0885328217748465 (2017).
7. Richmonds, C. et al. Electron-transfer reactions at the plasma-liquid interface. *J. Am. Chem. Soc.* **133**, 17582-17585, https://doi.org/10.1021/ja207547b (2011).
8. Bruggeman, P. J. et al. Plasma-liquid interactions: a review and roadmap. *Plasma Sources Sci. Technol.* **25**, 053002, https://doi.org/10.1088/0963-0252/25/5/053002 (2016).
9. Thai, P. V. et al. Interaction and transfer of charged particles from an alternating current glow discharge in liquids: Application to silver nanoparticle synthesis. *J. Appl. Phys.* **125**, 063303, https://doi.org/10.1063/1.5063872 (2019).
10. Heirman, P., Van Boxem, W. & Bogaerts, A. Reactivity and stability of plasma-generated oxygen and nitrogen species in buffered water solution: a computational study. *Phys. Chem. Chem. Phys.* **21**, 12881-12894, https://doi.org/10.1039/C9CP00647H (2019).
11. Lukes, P. & Locke, B. R. Plasmachemical oxidation processes in a hybrid gas–liquid electrical discharge reactor. *J. Phys. D: Appl. Phys.* **38**. 4074, https://doi.org/10.1088/0022-3727/38/22/010 (2005).

12. Sakakura, T., Murakami, N., Takatsuji, Y. & Haruyama, T. Nitrogen fixation in a plasma/liquid interfacial reaction and its switching between reduction and oxidation. *J. Phys. Chem. C* **124**, 9401-9408, https://doi.org/10.1021/acs.jpcc.0c02392 (2020).
13. Bhattacharyya, S. et al. Localized synthesis of metal nanoparticles using nanoscale corona discharge in aqueous solutions. *Adv. Mater.* **21**, 4039-4044, https://doi.org/10.1002/adma.200900673 (2009).
14. Amaliyah, N., Mukasa, S., Nomura, S., Toyota, H. & Kitamae, T. Plasma in-liquid method for reduction of zinc oxide in zinc nanoparticle synthesis. *Mater. Res. Express* **2**, 025004, https://doi.org/10.1088/2053-1591/2/2/025004 (2015).
15. Senthilnathan, J., Weng, C.-C., Liao, J.-D. & Yoshimura, M. Submerged liquid plasma for the synthesis of unconventional nitrogen polymers. *Sci. Rep.* **3**, 2414, https://doi.org/10.1038/srep02414 (2013).
16. Michael, P. et al. Plasma polymerized nanoparticles effectively deliver dual siRNA and drug therapy in vivo. *Sci. Rep.* **10**, 12836, https://doi.org/10.1038/s41598-020-69591-x (2020).
17. Pearse, R. W. B. & Gaydon, A. G. (1976) *The Identification of Molecular Spectra, Fourth Edition*, p.219, Chapman and Hall Ltd, London.
18. Bakolitsa, C. et al. Structural basis for vinculin activation at sites of cell adhesion. *Nature* **430**, 583-586, https://doi.org/10.1038/nature02610 (2004).
19. Sumpio, B. E., Riley, J. T. & Dardik, A. Cells in focus: endothelial cell. *Int. J. Biochem. Cell Biol.* **34**, 1508-1512, https://doi.org/10.1016/S1357-2725(02)00075-4 (2002).
20. Kusuma, S., Zhao, S. & Gerecht, S. The extracellular matrix is a novel attribute of endothelial progenitors and of hypoxic mature endothelial cells. *FASEB J.* **26**, 4925-4936, https://doi.org/10.1096/fj.12-209296 (2012).
21. Bourges-Monnier, C. & Shanahan, M. E. R. Influence of evaporation on contact angle. *Langmuir* **11**, 2820-2829, https://doi.org/10.1021/la00007a076 (1995).
22. Shen, C., Wen, Y., Kang, X. & Liu, W. H2O2-induced surface modification: A facile, effective and environmentally friendly pretreatment of chitosan for dyes removal. *Chem. Eng. J.* **166**, 474-482, https://doi.org/10.1016/j.cej.2010.10.075 (2011).
23. Din, I. U., Shaharun, M. S., Subbarao, D. & Naeem, A. Surface modification of carbon nanofibers by HNO_3 treatment. *Ceram. Int.* **42**, 966-970, https://doi.org/10.1016/j.ceramint.2015.08.054 (2016).
24. Hetemi, D. & Pinson, J. Surface functionalisation of polymers. *Chem. Soc. Rev.* **46**, 5701-5713, https://doi.org/10.1039/C7CS00150A (2017).

25. Nichols, E. L. & Clark, J. A. The influence of a static charge of electricity upon the surface tension of water. *Phys. Rev. (Series I)* **4**, 375-387, https://doi.org/10.1103/PhysRevSeriesI.4.375 (1897).
26. Bateni, A., Laughton, S., Tavana, H., Susnar, S. S., Amirfazli, A. & Neumann, A. W. Effect of electric fields on contact angle and surface tension of drops. *J. Colloid Interface Sci.* **283**, 215-222, https://doi.org/10.1016/j.jcis.2004.08.134 (2005).
27. Santos, L. P., Ducati, T. R. D., Balestrin, L. B. S. & Galembeck, F. Water with excess electric charge. J. Phys. Chem. C 115, 11226-11232, https://doi.org/10.1021/jp202652q (2011).
28. Szpak, P. Fish bone chemistry and ultrastructure: implications for taphonomy and stable isotope analysis. *J. Archaeol. Sci.* **38**, 3358-3372, https://doi.org/10.1016/j.jas.2011.07.022 (2011).
29. Jordan, T., Mukerji, I., Wang, Y. & Spiro, T. G. UV resonance Raman spectroscopy and hydrogen bonding of the proline peptide bond. *J. Mol. Struct.* **379**, 51-64, https://doi.org/10.1016/0022-2860(95)09162-9 (1996).
30. Zhang, Q. et al. Raman microspectroscopic and dynamic vapor sorption characterization of hydration in collagen and dermal tissue. *Biopolymers* **95**, 607-615, https://doi.org/10.1002/bip.21618 (2011).
31. Soto, C. A. T., Pereira, L., dos Santos, L., Rajasekaran, R., Fávero, P. & Martin, A. A. DFT:B3LYP/3-21G theoretical insights on the confocal Raman experimental observations in skin dermis of healthy young, healthy elderly, and diabetic elderly women. *J. Biomed. Opt.* **21**, 125002, https://doi.org/10.1117/1.JBO.21.12.125002 (2016).
32. Ali, S. M. In vivo confocal Raman spectroscopic imaging of the human skin extracellular matrix degradation due to accumulated intrinsic and extrinsic aging. *Photodermatol. Photoimmunol. Photomed.* **37**, 140-152, https://doi.org/10.1111/phpp.12623 (2021).
33. Nelson, D. L. & Cox, M. M. (2005) *Lehninger's Principles of Biochemistry, 4th Edition*, W. H. Freeman and Company, New York.
34. Brinckmann, J., Notbohm, H. & Müller, P. K. (2005) *Collagen, Topics in Current Chemistry 247*, Springer, Berlin.
35. Matulis, D. & Lovrien, R. 1-Anilino-8-Naphthalene Sulfonate Anion-Protein Binding Depends Primarily on Ion Pair Formation. *Biophys. J.* **74**, 422-429, https://doi.org/10.1016/S0006-3495(98)77799-9 (1998).

36. Friedrich, J. Mechanisms of plasma polymerization – reviewed from a chemical point of view. *Plasma Process. Polym.* 8, 783-802, https://doi.org/10.1002/ppap.201100038 (2011).
37. Mun, M. K., Jang, Y. J., Kim, J. E., Yeom, G. Y. & Kim D. W. Plasma functional polymerization of dopamine using atmospheric pressure plasma and a dopamine solution mist. *RSC Adv.* **9**, 12814-12822, https://doi.org/10.1039/C8RA10391G (2019).
38. Huang, Y.-H. & Wang, M.-J. Atmospheric pressure plasma jet-assisted copolymerization of sulfobetaine methacrylate and acrylic acid. *Plasma Process. Polym.* **17**, e1900209, https://doi.org/10.1002/ppap.201900209 (2020).
39. Schindelin, J. et al. Fiji: an open-source platform for biological-image analysis. *Nat. Methods* **9**, 676-682, https://doi.org/10.1038/nmeth.2019 (2012).
40. Li, X., Wang, R., Huang, S., Wang, Y. & Shi, H. A capillary rise method for studying the effective surface tension of monolayer nanoparticle-covered liquid marbles. *Soft Matter* **14**, 9877-9884, https://doi.org/10.1039/C8SM01846D (2018).
41. Ito, T., Obara, Y. & Misawa, K. Single-beam phase-modulated stimulated Raman scattering microscopy with spectrally focused detection. *J. Opt. Soc. Am. B* **34**, 1004-1015, https://doi.org/10.1364/JOSAB.34.001004 (2017).
42. Ito, T., Obara, Y. & Misawa, K. Invited Article: Spectral focusing with asymmetric pulses for high-contrast pump–probe stimulated Raman scattering microscopy. *APL Photonics* **3**, 092405, https://doi.org/10.1063/1.5030053 (2018).
43. Potocký, Š., Saito, N. & Takai, O. Needle electrode erosion in water plasma discharge. *Thin Solid Films* **518**, 918-923, https://doi.org/10.1016/j.tsf.2009.07.172 (2009).
44. Liu, Y., Li, Z., Luo, Q., Han, Y., Zhang, Q. & Lin, F. Comparison and evaluation of electrode erosion under high-pulsed current discharges in air and water mediums. IEEE Trans. Plasma Sci. 44, 1169-1177, https://doi.org/10.1109/TPS.2016.2578343 (2016).

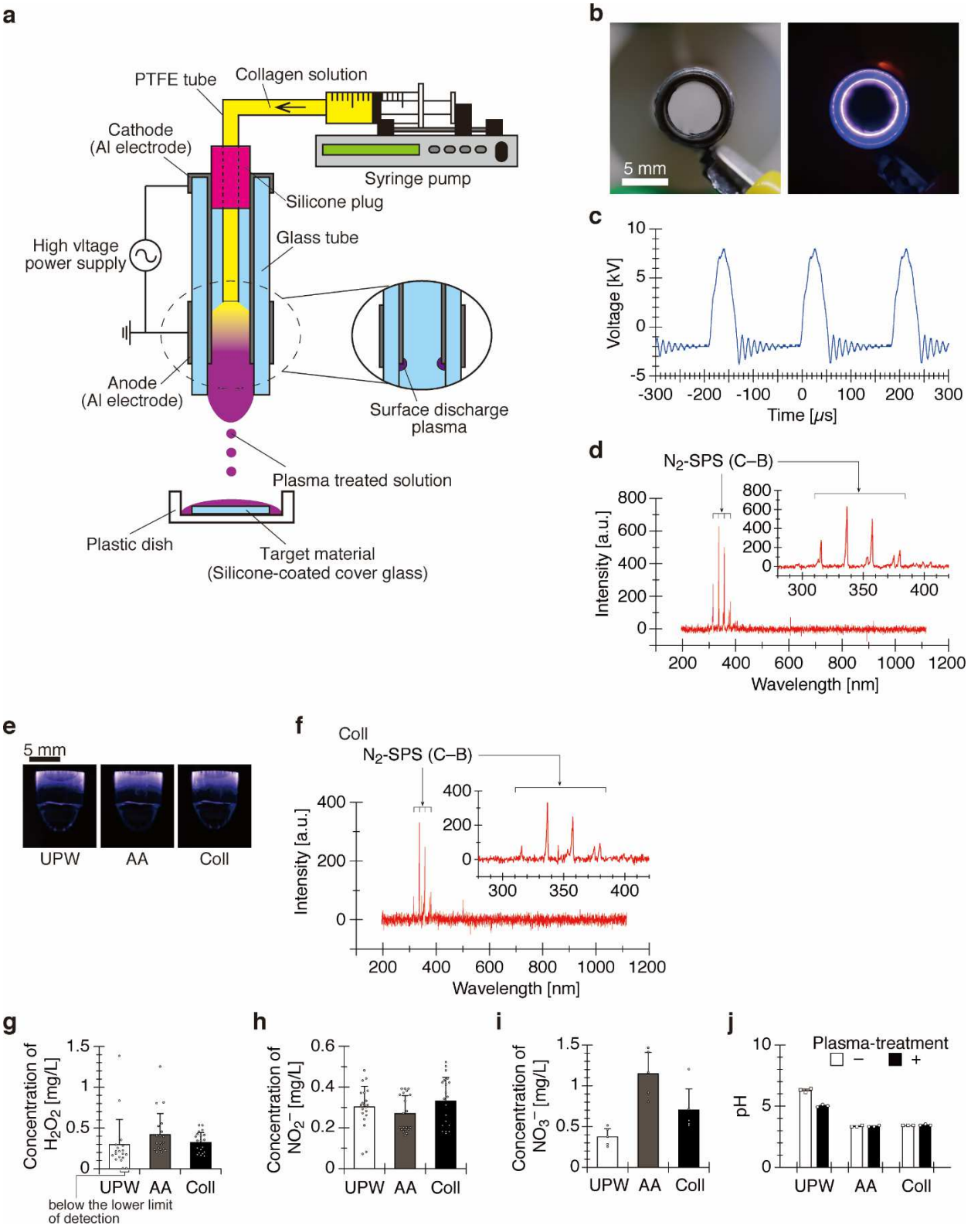

Fig. 1. Surface discharge plasma source. (a) Electrode design and the apparatus for plasma treatment of collagen solution. **(b)** Cross section of the electrode and light emitted by surface discharge plasma. **(c)** Waveform of the applied voltage. **(d)** Emission spectrum of plasma discharge in the gas phase. Typical peaks are attributed to the N_2-SPS(C–B). **(e)** Images of light emitted by the plasma generated in each solution. **(f)** Emission spectrum of

623 plasma discharge in the collagen solution. As in the case of discharge in the gas phase, a
624 peak typical of the N_2-SPS(C–B) was observed. Concentrations of dissolved **(g)** H_2O_2
625 (mean + SD, *n* = 20 experiments), **(h)** NO_2^- (mean + SD, *n* = 20 experiments), and **(i)** NO_3^-
626 (mean + SD, *n* = 5 experiments) in each solution after plasma treatment. **(j)** Change in pH
627 of each solution before and after plasma treatment (mean + SD, *n* = 3 experiments). UPW,
628 ultrapure water; AA, 20 mM acetic acid; Coll, 50 μg/mL collagen solution.

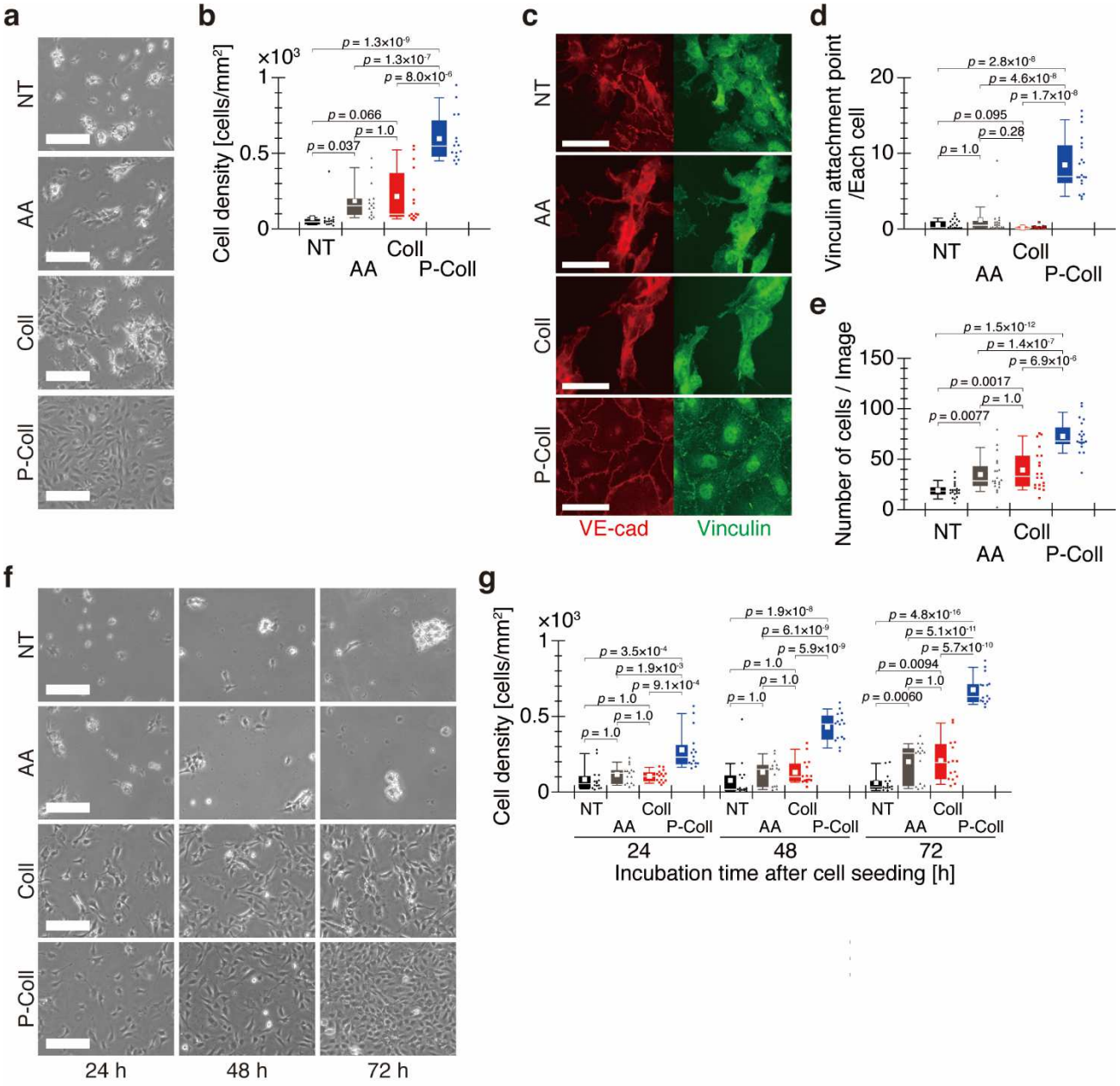
a
NT
AA
Coll
P-Coll
b
Cell density [cells/mm²]
×10³
1
0.5
0
p = 1.3×10⁻⁹
p = 1.3×10⁻⁷
p = 8.0×10⁻⁶
p = 0.066
p = 1.0
p = 0.037
NT
Coll
AA
P-Coll
c
NT
AA
Coll
P-Coll
VE-cad
Vinculin
d
Vinculin attachment point /Each cell
20
10
0
p = 2.8×10⁻⁸
p = 4.6×10⁻⁸
p = 1.7×10⁻⁸
p = 0.095
p = 0.28
p = 1.0
NT
Coll
AA
P-Coll
e
Number of cells / Image
150
100
50
0
p = 1.5×10⁻¹²
p = 1.4×10⁻⁷
p = 6.9×10⁻⁶
p = 0.0017
p = 1.0
p = 0.0077
NT
Coll
AA
P-Coll
f
NT
AA
Coll
P-Coll
24 h
48 h
72 h
g
Cell density [cells/mm²]
×10³
1
0.5
0
p = 3.5×10⁻⁴
p = 1.9×10⁻³
p = 9.1×10⁻⁴
p = 1.0
p = 1.0
p = 1.0
p = 1.9×10⁻⁸
p = 6.1×10⁻⁹
p = 5.9×10⁻⁹
p = 1.0
p = 1.0
p = 1.0
p = 4.8×10⁻¹⁶
p = 5.1×10⁻¹¹
p = 5.7×10⁻¹⁰
p = 0.0094
p = 1.0
p = 0.0060
NT
Coll
AA
P-Coll
24
48
72
Incubation time after cell seeding [h]
h
NT
AA
Coll
P-Coll
VE-cad
Vinculin
i
Vinculin attachment point /Each cell
30
20
10
0
p = 9.9×10⁻⁵
p = 2.8×10⁻⁵
p = 1.7×10⁻⁵
p = 1.0
p = 1.0
p = 1.0
NT
Coll
AA
P-Coll
j
Number of cells / Image
150
100
50
0
p = 8.6×10⁻⁹
p = 2.3×10⁻⁷
p = 4.4×10⁻¹¹
p = 1.0
p = 0.012
p = 0.159
NT
Coll
AA
P-Coll

Fig. 2. Biofunctionalization of silicone-coated hydrophobic cover glass with plasma-treated collagen solution. (a) Adhesion of endothelial cells on hydrophobic cover glass pre-coated with each solution. Scale bars, 200 μm. **(b)** Number of adhered HUVECs in a 1-mm^2 area 24 h after seeding. Whiskers represent the 10th and 90th percentiles, the box represents the 25th to 75th percentiles, the central line depicts the median, and the white square inside each box indicates the average value. Each value was obtained from 15 images, which were captured from three independently repeated experiments (*n* = 15 images). **(c)** Representative fluorescence images of VE-cadherin and vinculin in adherent cells 24 h after seeding. Scale bars, 50 μm. **(d)** Quantification of vinculin attachment points in an adherent cell calculated based on **(e)** the number of cells in each image. Each value is shown as a box-and-whisker plot obtained from 20 images in three independently repeated experiments (*n* = 20 images). **(f)** Proliferation of HUVECs on hydrophobic cover glass pre-coated with each solution. Scale bars, 200 μm. **(g)** Number of HUVECs in a 1-mm^2 area 24 to 72 h after seeding. Each value is shown as a box-and-whisker plot obtained from 15 images in three independently repeated experiments (*n* = 15 images). **(h)** Representative fluorescence images of VE-cadherin and vinculin in cells proliferating on hydrophobic cover glass 72 h after seeding. Scale bars, 50 μm. **(i)** Quantification of vinculin attachment points in a proliferated cell calculated based on **(j)** the number of cells in each image. Each value is shown as a box-and-whisker plot obtained from 20 images in three independently repeated experiments (*n* = 20 images). NT, non-treated; AA, 20 mM acetic acid; Coll, 50 μg/mL collagen solution; P-Coll, plasma-treated collagen solution.

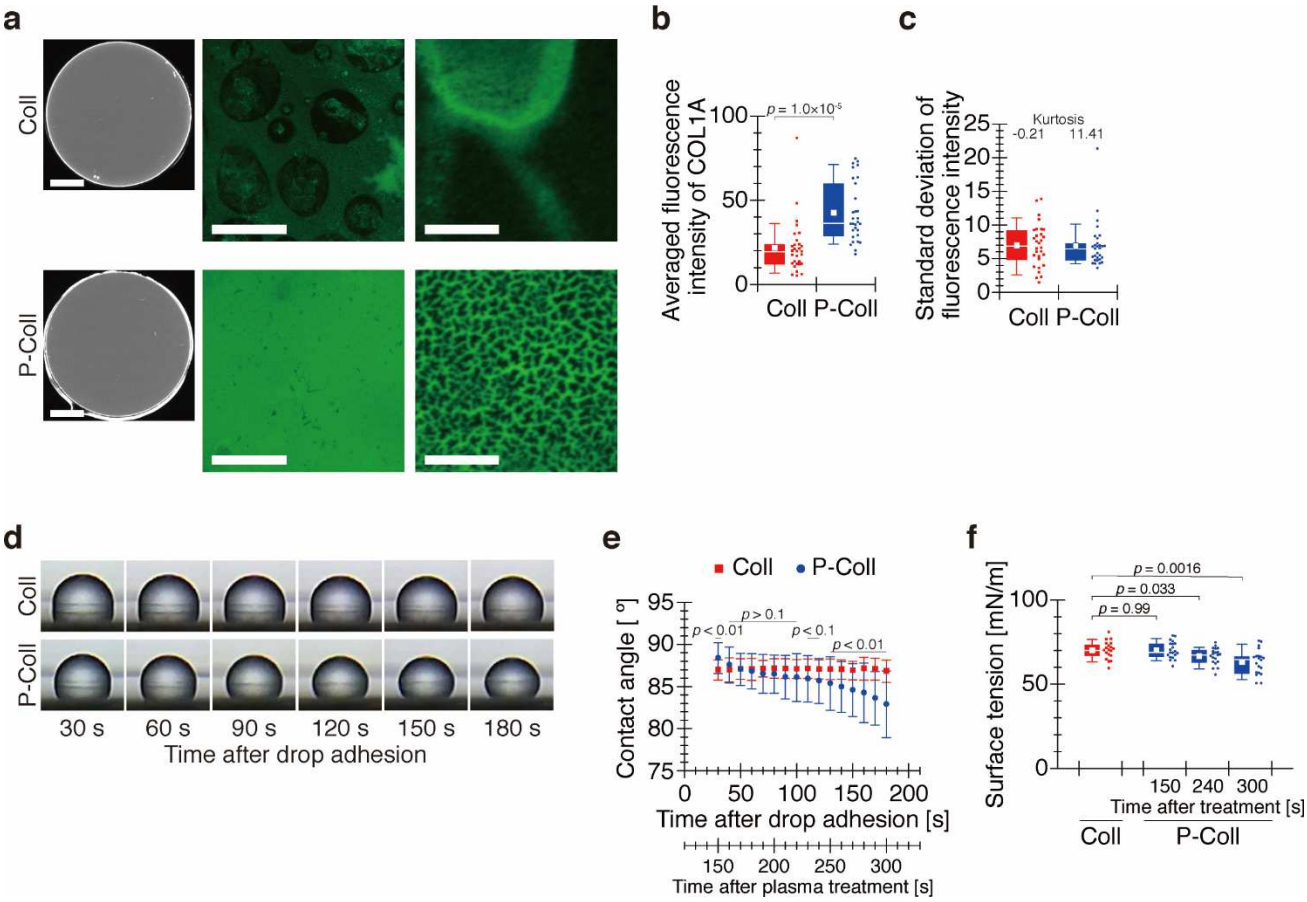

Fig. 3. Collagen coating quality derives from plasma-induced changes in surface and interfacial properties and contributes to substrate biofunctionalization. (a) Representative fluorescence images of collagen (COL1A) on hydrophobic cover glass. Scale bars, 5 mm (*left*), 50 µm (*middle*), and 10 µm (*right*). **(b, c)** Quantification of coating quality. **(b)** Averaged fluorescence intensity and **(c)** standard deviation of fluorescence intensity of COL1A in a rectangular region (240 × 240 µm). Each value is shown as a box-and-whisker plot obtained from 30 images in six independently repeated experiments (*n* = 30 images). **(d)** Time sequence images of a collagen solution droplet on hydrophobic cover glass. **(e)** Temporal change in contact angle of the collagen solution droplet (mean ± SD, *n* = 20 experiments). **(f)** Variation over time of surface tension of the collagen solution. Each value is shown as a box-and-whisker plot obtained from 20 independently repeated experiments (*n* = 20 experiments). Coll, 50 µg/mL collagen solution; P-Coll, plasma-treated collagen solution.

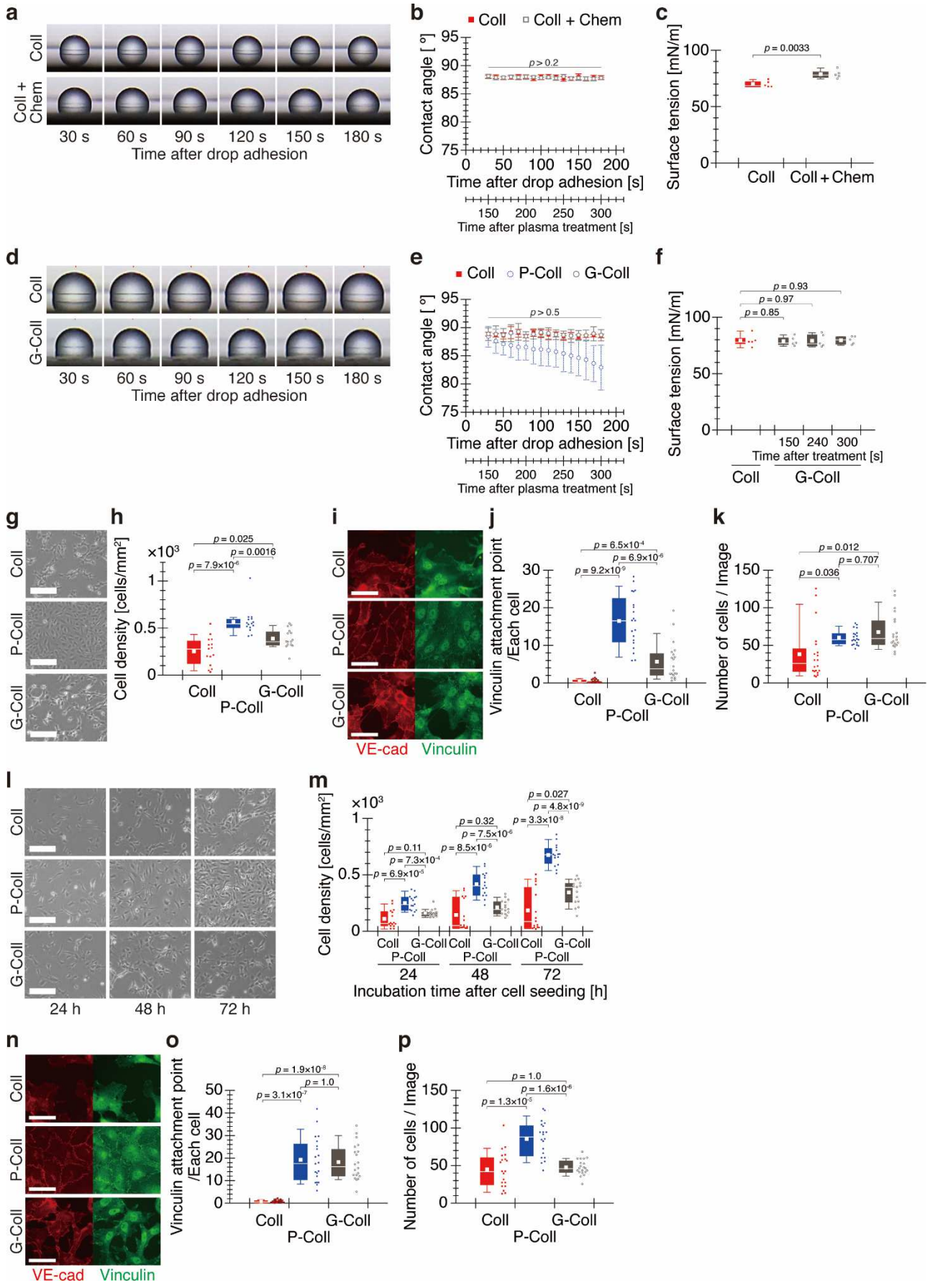
a
Coll
Coll + Chem
30 s
60 s
90 s
120 s
150 s
180 s
Time after drop adhesion
b
Coll
Coll + Chem
Contact angle [°]
p > 0.2
Time after drop adhesion [s]
Time after plasma treatment [s]
c
Surface tension [mN/m]
p = 0.0033
Coll
Coll + Chem
d
Coll
G-Coll
30 s
60 s
90 s
120 s
150 s
180 s
Time after drop adhesion
e
Coll
P-Coll
G-Coll
Contact angle [°]
p > 0.5
Time after drop adhesion [s]
Time after plasma treatment [s]
f
Surface tension [mN/m]
p = 0.93
p = 0.97
p = 0.85
Time after treatment [s]
Coll
G-Coll
g
Coll
P-Coll
G-Coll
h
Cell density [cells/mm²]
p = 0.025
p = 0.0016
p = 7.9×10⁻⁶
Coll
G-Coll
P-Coll
i
Coll
P-Coll
G-Coll
VE-cad
Vinculin
j
Vinculin attachment point /Each cell
p = 6.5×10⁻⁴
p = 6.9×10⁻⁶
p = 9.2×10⁻⁹
Coll
G-Coll
P-Coll
k
Number of cells / Image
p = 0.012
p = 0.707
p = 0.036
Coll
G-Coll
P-Coll
l
Coll
P-Coll
G-Coll
24 h
48 h
72 h
m
Cell density [cells/mm²]
p = 0.11
p = 7.3×10⁻⁴
p = 6.9×10⁻⁵
p = 0.32
p = 7.5×10⁻⁶
p = 8.5×10⁻⁶
p = 0.027
p = 4.8×10⁻⁹
p = 3.3×10⁻⁸
Coll
G-Coll
P-Coll
24
48
72
Incubation time after cell seeding [h]
n
Coll
P-Coll
G-Coll
VE-cad
Vinculin
o
Vinculin attachment point /Each cell
p = 1.9×10⁻⁸
p = 1.0
p = 3.1×10⁻⁷
Coll
G-Coll
P-Coll
p
Number of cells / Image
p = 1.0
p = 1.6×10⁻⁶
p = 1.3×10⁻⁵
Coll
G-Coll
P-Coll

665

Fig. 4. Electric charge regulates the surface and interfacial properties of the solution, leading to substrate biofunctionalization. (a) Time sequence images of a droplet of collagen solution containing chemical species on hydrophobic cover glass. **(b)** Contact angle of a droplet of collagen solution containing chemical species (mean ± SD, *n* = 5 experiments). **(c)** Temporal variation of the surface tension of collagen solution containing chemical species. Each value is shown as a box-and-whisker plot obtained from five independently repeated experiments (*n* = 5 experiments). **(d)** Time sequence images of a collagen solution droplet on hydrophobic cover glass. **(e)** Contact angle of a droplet of collagen solution in which the charge was released after plasma treatment (mean ± SD, *n* = 5 experiments). **(f)** Temporal variation of the surface tension of collagen solution in which the charge was released after plasma treatment. Each value is shown as a box-and-whisker plot obtained from five independently repeated experiments (*n* = 5 experiments). **(g)** Phase-contrast images of HUVECs adhered onto hydrophobic cover glass pre-coated with each solution. Scale bars, 200 μm. **(h)** Number of adherent HUVECs in a 1-mm^2 area 24 h after seeding. Each value is shown as a box-and-whisker plot obtained from 15 images in three independently repeated experiments (*n* = 15 images). **(i)** Representative fluorescence images of VE-cadherin and vinculin in adherent cells 24 h after seeding. Scale bars, 50 μm. **(j)** Quantification of vinculin attachment points in an adherent cell calculated based on **(k)** the number of cells in each image. Each value is shown as a box-and-whisker plot obtained from 20 images in three independently repeated experiments (*n* = 20 images). **(l)** Phase-contrast images of cell proliferation on hydrophobic cover glass pre-coated with each solution. Scale bars, 200 μm. **(m)** Number of HUVECs in a 1-mm^2 area 24 to 72 h after seeding. Each value is shown as a box-and-whisker plot obtained from 15 images in three independently repeated experiments (*n* = 15 images). **(n)** Representative fluorescence images of VE-cadherin and vinculin in cells proliferating on hydrophobic cover glass 72 h after seeding. Scale bars, 50 μm. **(o)** Quantification of vinculin attachment points in a proliferated cell calculated based on **(p)** the number of cells in each image. Each value is shown as a box-and-whisker plot obtained from 20 images in three independently repeated experiments (*n* = 20 images). Coll, 50 μg/mL collagen solution; Coll + Chem, collagen solution containing H_2O_2, NO_2^-, and NO_3^- at concentrations equal to those produced by plasma treatment; P-Coll, plasma-treated collagen solution; G-Coll, collagen solution in which the charge was released after plasma treatment.

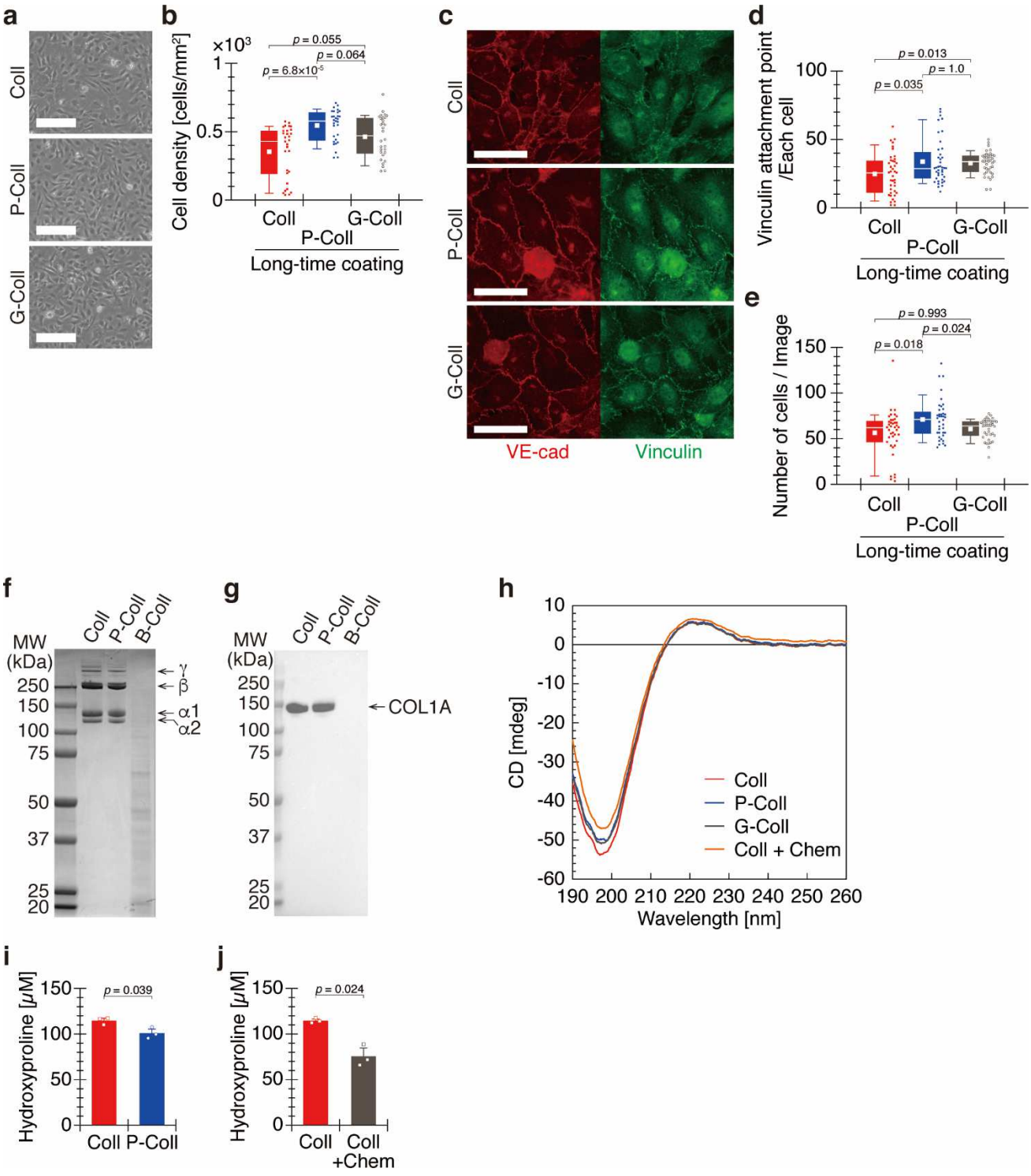

Fig. 5. Coating for an extended period enhances biofunctionalization regardless of the charge state of the collagen solution, but plasma treatment does not cause thermal denaturation or significant structural changes in collagen. (a) HUVECs adhering onto hydrophobic cover glass pre-coated with each solution for 1 h. Scale bars, 200 μm. **(b)** Number of adherent HUVECs in a 1-mm^2 area 24 h after seeding. Each value is shown as a box-and-whisker plot obtained from 15 images in three independently repeated experiments (n = 15 images). **(c)** Representative fluorescence images of VE-

cadherin and vinculin in HUVECs 24 h after seeding. Scale bars, 50 μm. **(d)** Quantification of vinculin attachment points in a cell calculated based on **(e)** the number of cells in each image. Each value is shown as a box-and-whisker plot obtained from 20 images in three independently repeated experiments (*n* = 20 images). **(f)** Representative CBB-stained electrophoresis gel of collagen molecules in solution and **(g)** representative blot of COL1A. Images are representative of three independent experiments with similar results (*n* = 3 experiments). **(h)** Averaged circular dichroism spectra of collagen solution (*n* = 5 experiments). **(i, j)** Amount of hydroxyproline in each collagen solution (*n* = 3 experiments). Coll, 50 μg/mL collagen solution; P-Coll, plasma-treated collagen solution; G-Coll, collagen solution in which the charge was released after plasma treatment; B-Coll, collagen solution boiled for 1 h; Coll + Chem, collagen solution containing H_2O_2, NO_2^-, and NO_3^- at concentrations equal to those produced by plasma treatment.

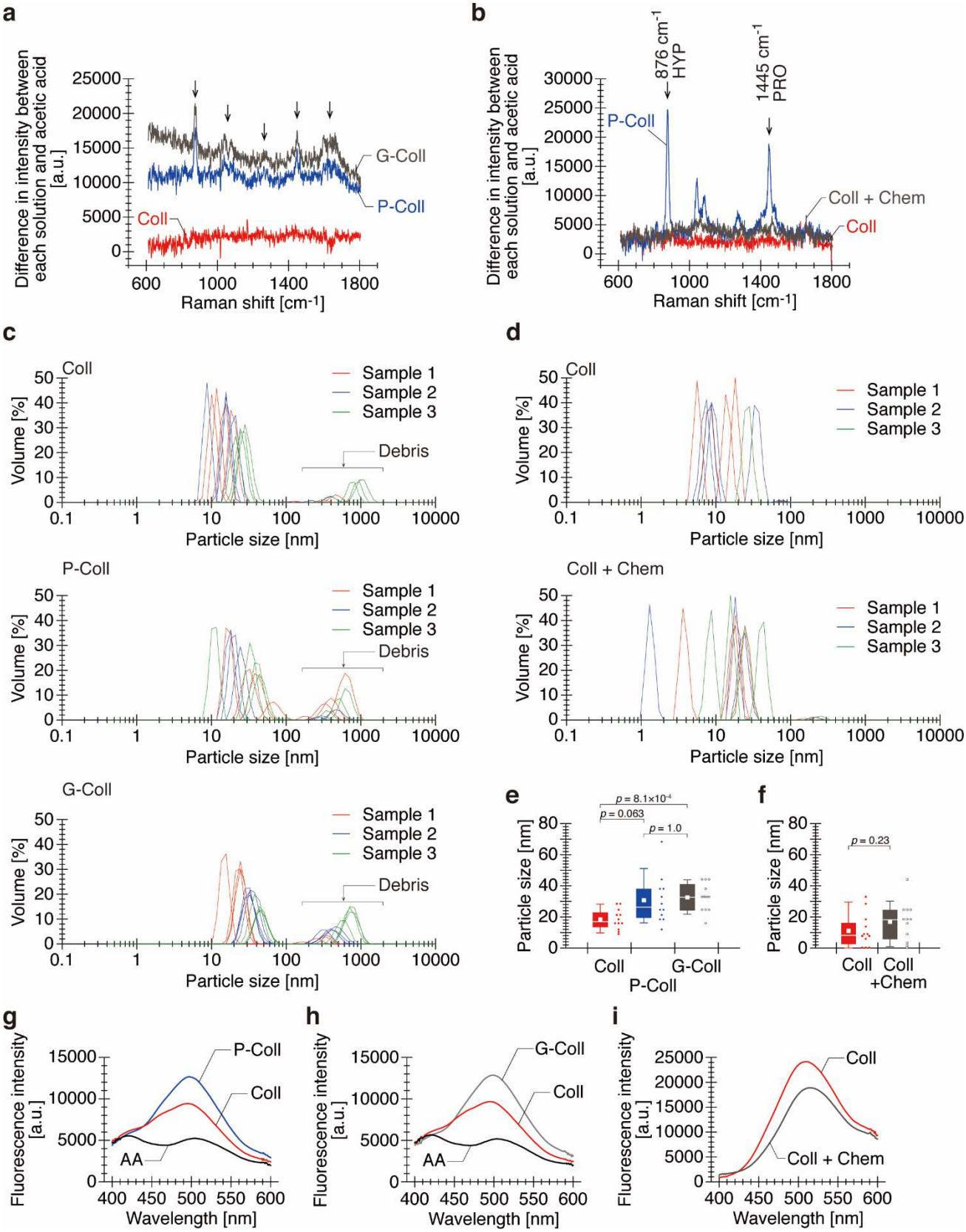

Fig. 6. Plasma induces changes in the local conformation and association state of collagen molecules, leading to biofunctionalization of hydrophobic substrates. (a, b) Difference in Raman spectra intensity between each solution and 20 mM acetic acid. Data

shown are representative of three independent experiments with similar results (*n* = 3 experiments). HYP, hydroxyproline; PRO, proline. **(c, d)** Size distribution of collagen associations in each solution. **(e, f)** Peak size of collagen associations extracted from 12 measurement results based on three independent samples (*n* = 12 measurement results). Peak values were evaluated excluding particles >100 nm in size, which represent plasma discharge–related debris originating from the electrodes. **(g, h, i)** Averaged ANS-fluorescence intensity in collagen solution (*n* = 6 measurement results; **g**, **h**, and *n* = 7 measurement results, **i**). Coll, 50 μg/mL collagen solution; P-Coll, plasma-treated collagen solution; G-Coll, collagen solution in which the charge was released after plasma treatment. Coll + Chem, collagen solution containing H_2O_2, NO_2^-, and NO_3^- at concentrations equal to those produced by plasma treatment.

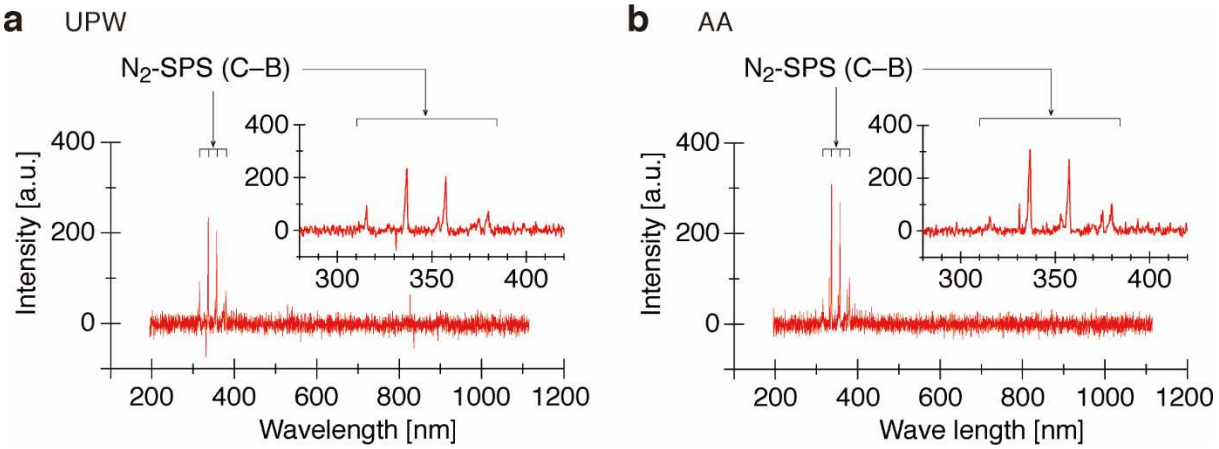

Supplementary Fig. 1. Emission spectra of plasma discharge in each solution. (a) Ultrapure water (UPW) and **(b)** 20 mM acetic acid (AA). The typical peaks are attributed to the N_2-SPS(C–B).

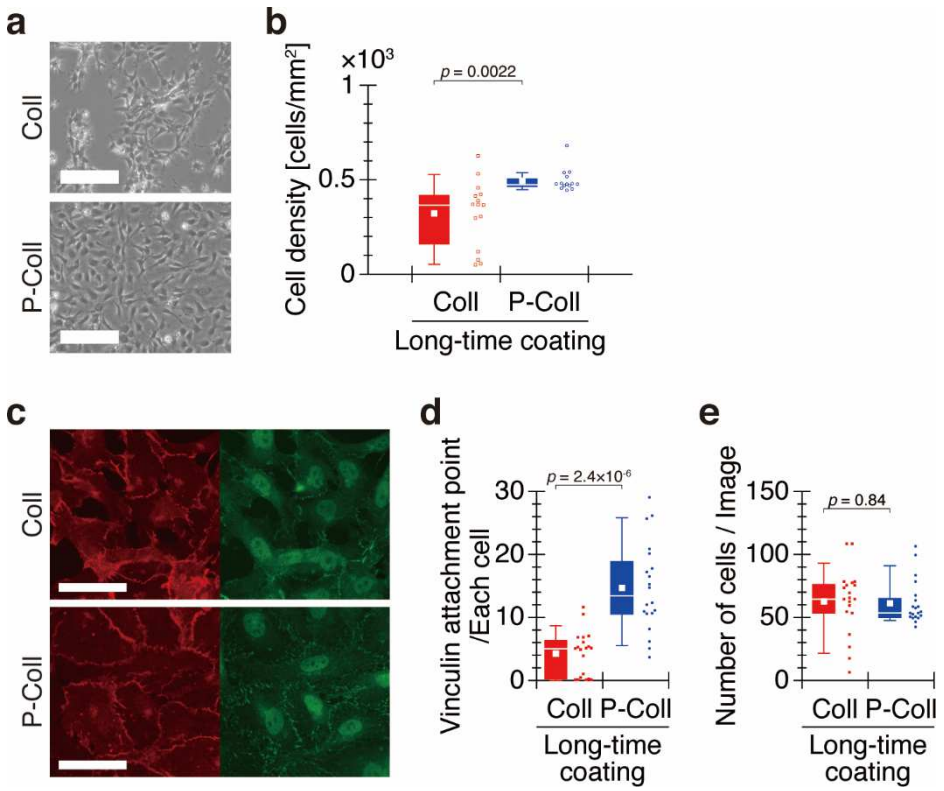

Supplementary Fig. 2. Effect of coating with plasma-treated collagen solution for an extended period of time on biofunctionalization of a hydrophobic cover glass. (a) Adhesion of endothelial cells onto hydrophobic cover glass pre-coated with collagen solution for 1 h. Scale bars, 200 μm. **(b)** Number of adhered HUVECs in a 1-mm^2 area 24 h after seeding. Whiskers represent the 10th and 90th percentiles, the box represents the 25th to 75th percentiles, the central line depicts the median, and the white square inside each box indicates the average value. Each value was obtained from 15 images captured from three independently repeated experiments (*n* = 15 images). **(c)** Representative fluorescence images of VE-cadherin and vinculin in adherent cells 24 h after seeding. Scale bars, 50 μm. **(d)** Quantification of vinculin attachment points in an adherent cell calculated based on **(e)** the number of cells in each image. Each value is shown as a box-and-whisker plot obtained from 20 images in three independently repeated experiments (*n* = 20 images). Coll, 50 μg/mL collagen solution; P-Coll, plasma-treated collagen solution.

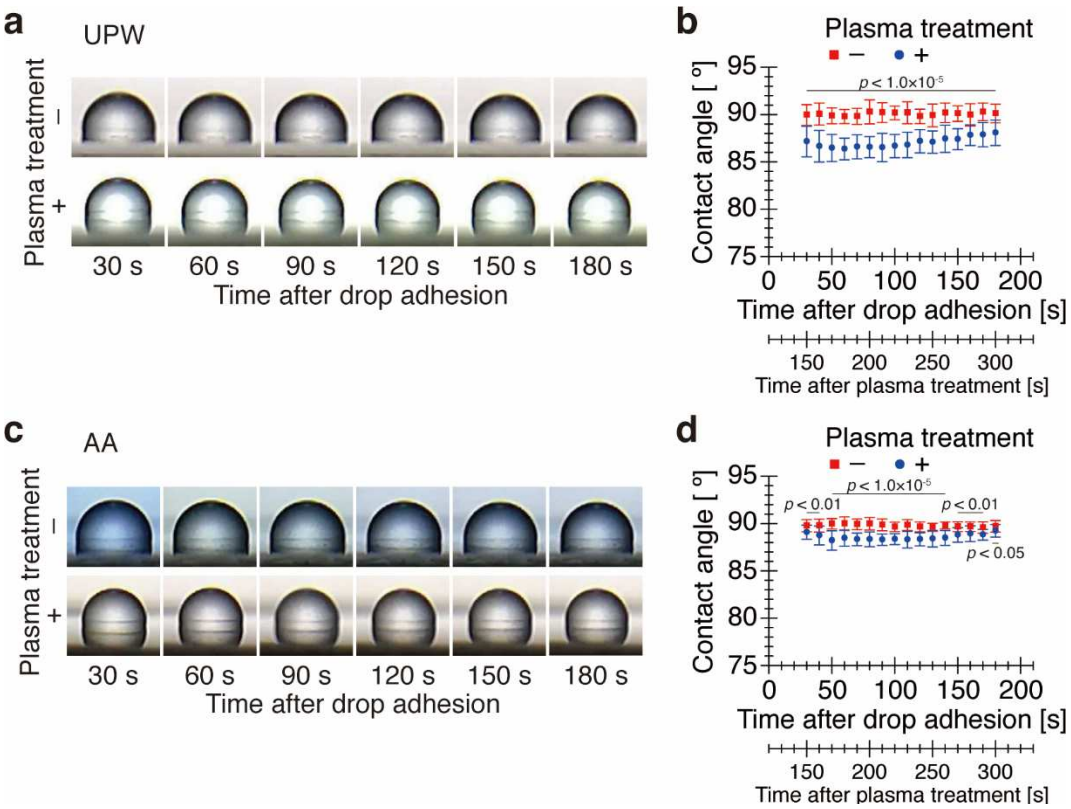

Supplementary Fig. 3. Plasma induces transient changes in interfacial properties between the hydrophobic substrate and the solution. (a) Time sequence images of an ultrapure water (UPW) droplet on hydrophobic cover glass. **(b)** Temporal variation of the contact angle of an UPW droplet (mean ± SD, *n* = 20 experiments). **(c)** Time sequence images of a 20 mM acetic acid (AA) droplet on hydrophobic cover glass. **(d)** Temporal variation of the contact angle of an AA droplet (mean ± SD, *n* = 20 experiments).

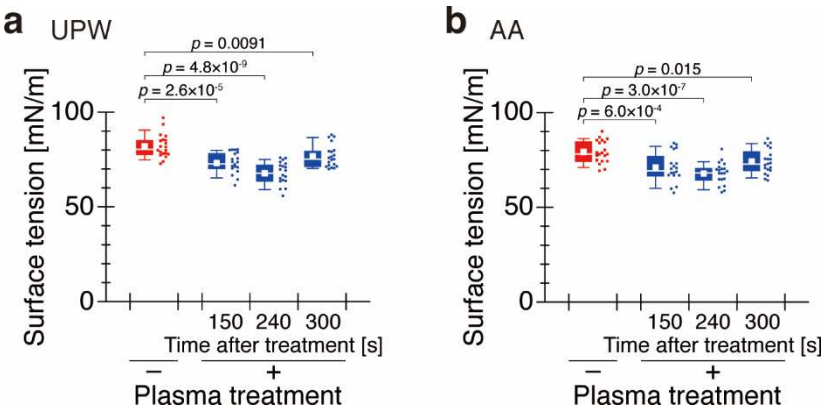

Supplementary Fig. 4. Plasma induces transient changes in surface properties of the solution. Temporal variation of the surface tension of **(a)** ultrapure water (UPW) and **(b)** 20 mM acetic acid (AA). Whiskers represent the 10th and 90th percentiles, the box represents the 25th to 75th percentiles, the central line depicts the median, and the white square inside each box indicates the average value. Each value was obtained from 20 independently repeated experiments (*n* = 20 experiments).

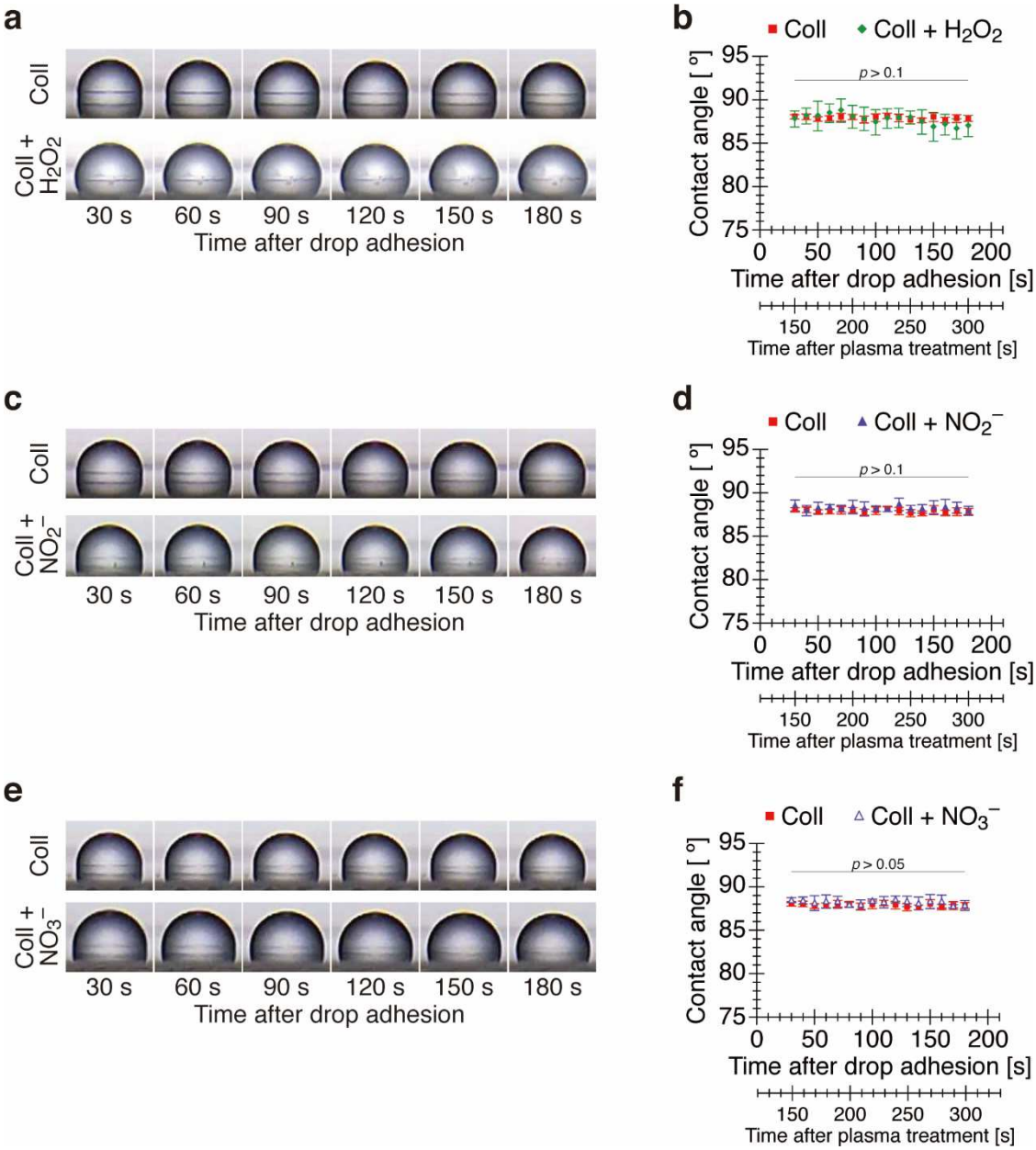

765

766 **Supplementary Fig. 5. Chemical species cause no change in interfacial properties**
767 **between the hydrophobic substrate and collagen solution.** Time sequence images of a
768 droplet of 50 μg/mL collagen solution containing **(a)** H_2O_2, **(c)** NO_2^-, or **(e)** NO_3^- on
769 hydrophobic cover glass. Contact angle of a droplet of 50 μg/mL collagen solution
770 containing **(b)** H_2O_2, **(d)** NO_2^-, or **(f)** NO_3^- (mean ± SD, n = 5 experiments).

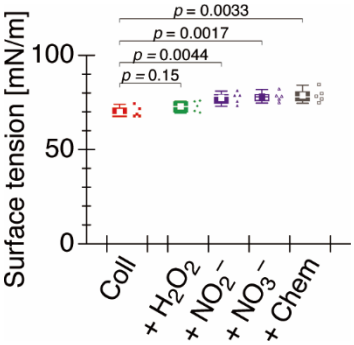

Supplementary Fig. 6. Chemical species do not change the surface properties of collagen solution resulting from plasma treatment. Surface tension of 50 μg/mL collagen solution containing chemical species. Whiskers represent the 10th and 90th percentiles, the box represents the 25th to 75th percentiles, the central line depicts the median, and the white square inside each box indicates the average value. Each value was obtained from five independently repeated experiments (*n* = 5 experiments). Coll + Chem, collagen solution containing H_2O_2, NO_2^-, and NO_3^- at concentrations equal to those produced by plasma treatment.

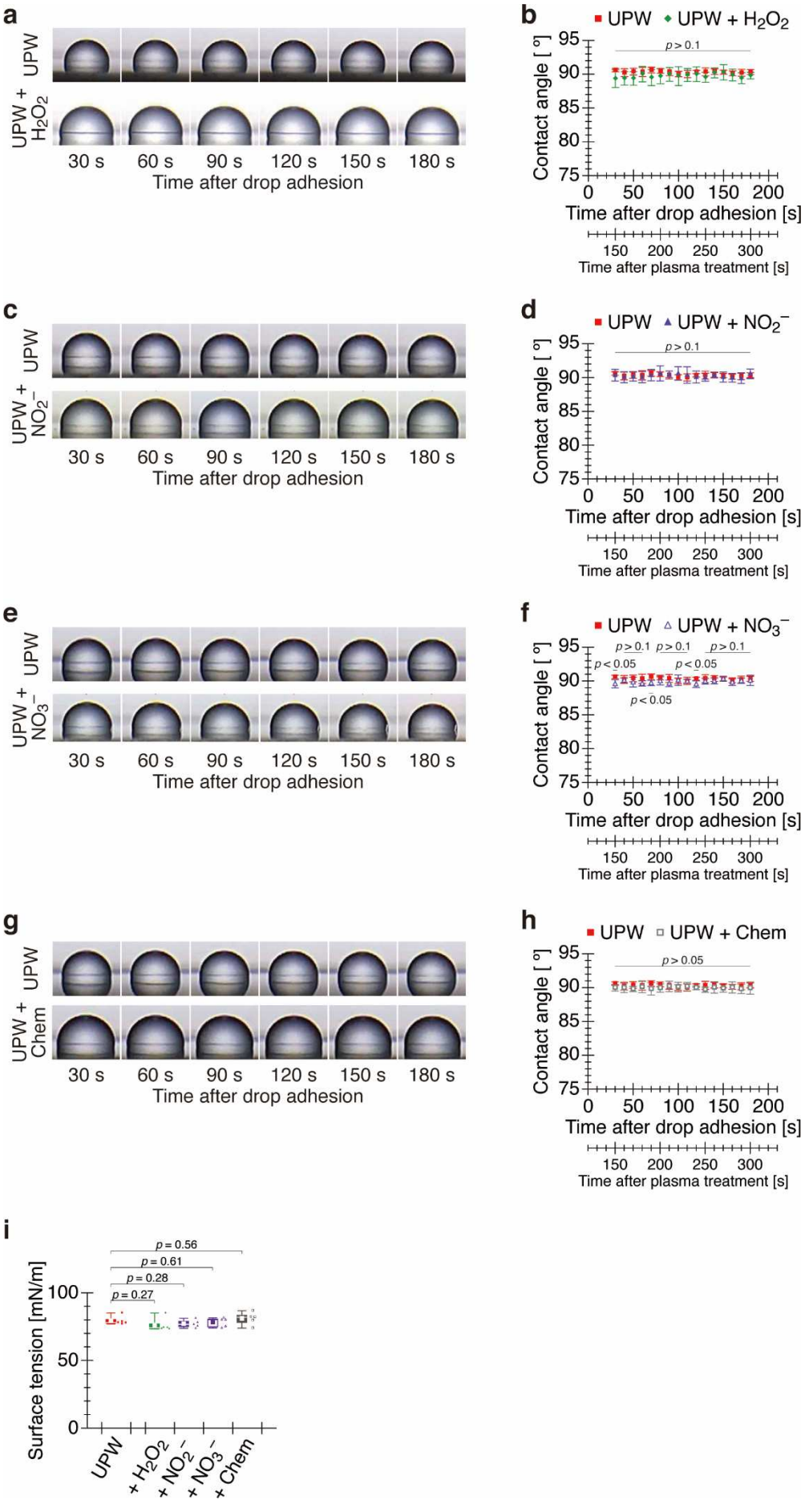
a
UPW
UPW + H2O2
30 s
60 s
90 s
120 s
150 s
180 s
Time after drop adhesion
b
UPW
UPW + H2O2
p > 0.1
Contact angle [°]
Time after drop adhesion [s]
Time after plasma treatment [s]
c
UPW
UPW + NO2−
d
e
UPW
UPW + NO3−
f
p < 0.05
g
UPW
UPW + Chem
h
p > 0.05
i
p = 0.56
p = 0.61
p = 0.28
p = 0.27
Surface tension [mN/m]
UPW
+ H2O2
+ NO2−
+ NO3−
+ Chem

Supplementary Fig. 7. Chemical species cause no changes in surface and interfacial properties of ultrapure water (UPW). Time sequence images of a droplet of UPW containing **(a)** H_2O_2, **(c)** NO_2^-, or **(e)** NO_3^- on hydrophobic cover glass. Contact angle of a droplet of UPW containing **(b)** H_2O_2, **(d)** NO_2^-, or **(f)** NO_3^- (mean ± SD, *n* = 5 experiments). **(i)** Surface tension of UPW containing chemical species. Whiskers represent the 10th and 90th percentiles, the box represents the 25th to 75th percentiles, the central line depicts the median, and the white square inside each box indicates the average value. Each value was obtained from five independently repeated experiments (*n* = 5 experiments). UPW + Chem, UPW containing H_2O_2, NO_2^-, and NO_3^- at concentrations equal to those produced by plasma treatment.

a

No.	Viscosity [mPa•s]	
	Coll	P-Coll
1	1.02 (24.0 °C)	1.07 (23.5 °C)
2	1.05 (23.6 °C)	1.05 (23.8 °C)
3	1.02 (24.3 °C)	1.04 (24.2 °C)
4	1.00 (24.0 °C)	1.02 (24.3 °C)
5	1.00 (24.3 °C)	1.02 (24.2 °C)
6	1.00 (24.3 °C)	1.02 (24.4 °C)
7	1.02 (24.1 °C)	1.04 (24.3 °C)
8	1.00 (25.0 °C)	1.04 (24.8 °C)
9	1.02 (25.0 °C)	1.02 (25.0 °C)
10	1.00 (25.2 °C)	1.02 (25.1 °C)

b

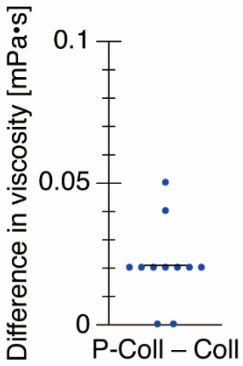

c

No.	Viscosity [mPa•s]			
	Coll	P-Coll	Coll	G-Coll
1	1.00 (25.4 °C)	1.02 (25.3 °C)	1.00 (22.8 °C)	1.02 (22.7 °C)
2	1.04 (22.4 °C)	1.05 (22.4 °C)	1.00 (22.8 °C)	1.02 (22.7 °C)
3	1.02 (22.4 °C)	1.03 (22.3 °C)	1.02 (22.7 °C)	1.02 (22.8 °C)
4	1.04 (22.5 °C)	1.04 (22.4 °C)	1.02 (23.1 °C)	1.02 (23.2 °C)
5	1.04 (22.4 °C)	1.05 (22.3 °C)	1.02 (22.7 °C)	1.02 (22.8 °C)
6	1.00 (21.9 °C)	1.04 (21.9 °C)	1.02 (22.4 °C)	1.04 (22.4 °C)
7	1.02 (22.3 °C)	1.02 (22.3 °C)	1.02 (22.1 °C)	1.04 (22.1 °C)
8	1.02 (22.3 °C)	1.05 (22.1 °C)	1.00 (22.6 °C)	1.02 (22.5 °C)
9	1.04 (21.5 °C)	1.05 (21.6 °C)	1.02 (22.4 °C)	1.02 (22.4 °C)
10	1.02 (21.7 °C)	1.04 (21.8 °C)	1.02 (22.5 °C)	1.02 (22.6 °C)

d

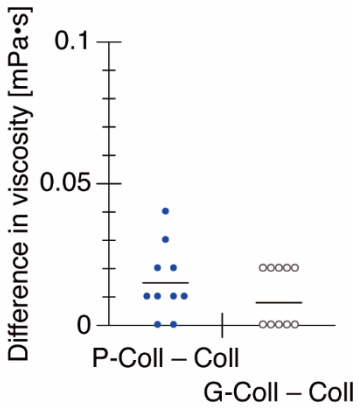

Supplementary Fig. 8. Plasma treatment induces a slight increase in the viscosity of collagen solution. (a) Viscosity of collagen solution before and after plasma treatment. **(b)** Difference in the viscosity of collagen solution before and after plasma treatment (*n* = 10 experiments). **(c)** Viscosity of collagen solution under various conditions. **(d)** Difference in the viscosity of collagen solution before and after plasma treatment (*n* = 10 experiments). Slight increase in viscosity was also observed in collagen solution in which the charge was released after plasma treatment. Coll, 50 μg/mL collagen solution; P-Coll, plasma-treated collagen solution; G-Coll, collagen solution in which the charge was released after plasma treatment.

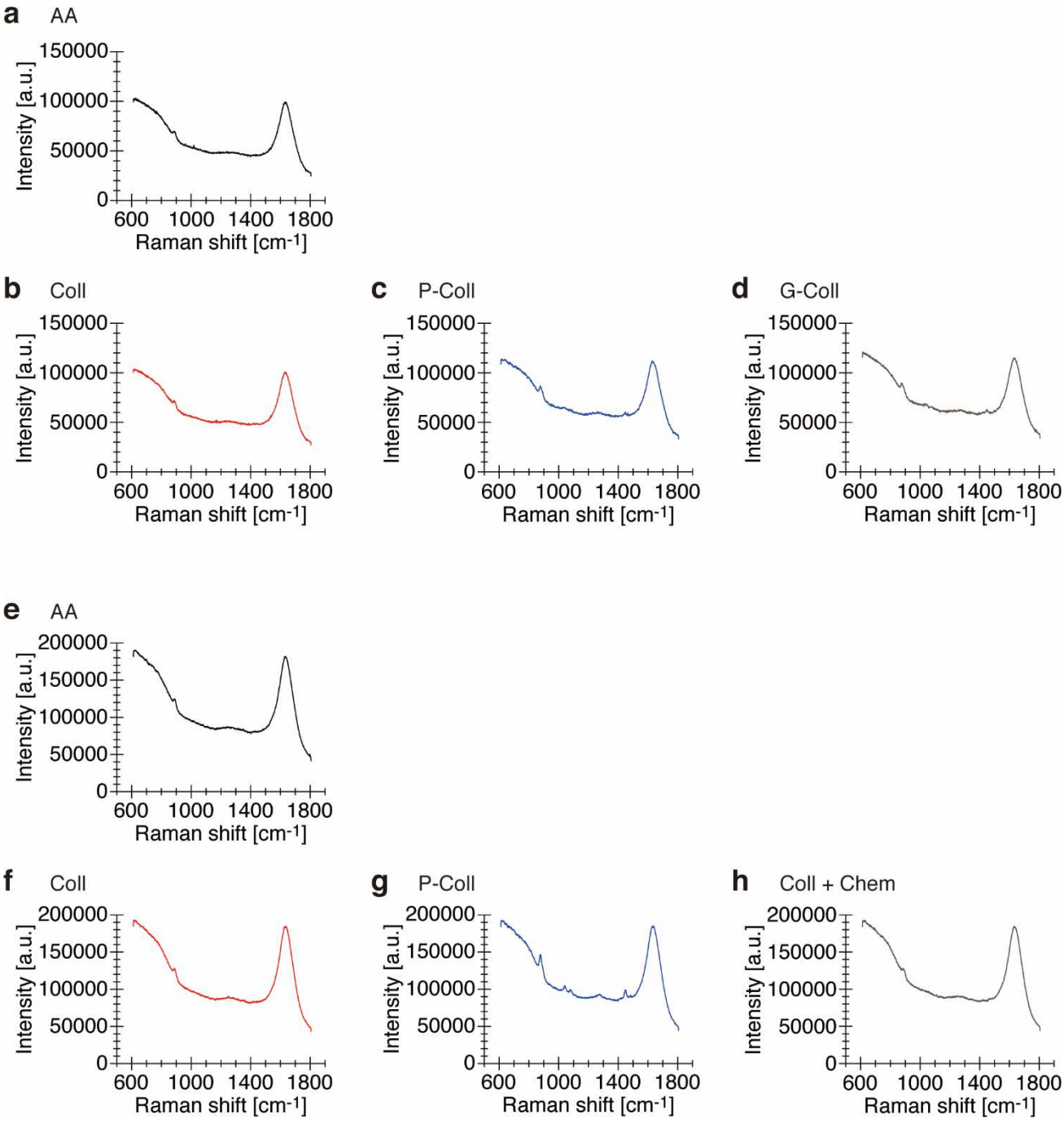

Supplementary Fig. 9. Raman spectral waveform of collagen solution under various conditions. (a) 20 mM acetic acid solution (AA) as base. **(b)** 50 μg/mL collagen solution (Coll). **(c)** Collagen solution after plasma treatment (P-Coll). **(d)** Collagen solution in which the charge was released after plasma treatment (G-Coll). **(e)** 20 mM AA solution as base. **(f)** 50 μg/mL Coll. **(g)** Collagen solution after plasma treatment (P-Coll). **(h)** Collagen solution containing H_2O_2, NO_2^-, and NO_3^- at concentrations equal to those produced by plasma treatment (Coll + Chem). These Raman spectral waveforms were used to calculate the difference in Raman intensities (**Fig. 6a** and **b**) **Fig. 6a** was derived from **Supplementary Fig. 9a-d**. **Supplementary Fig. 9e-h** served as source data for **Fig. 6b**.

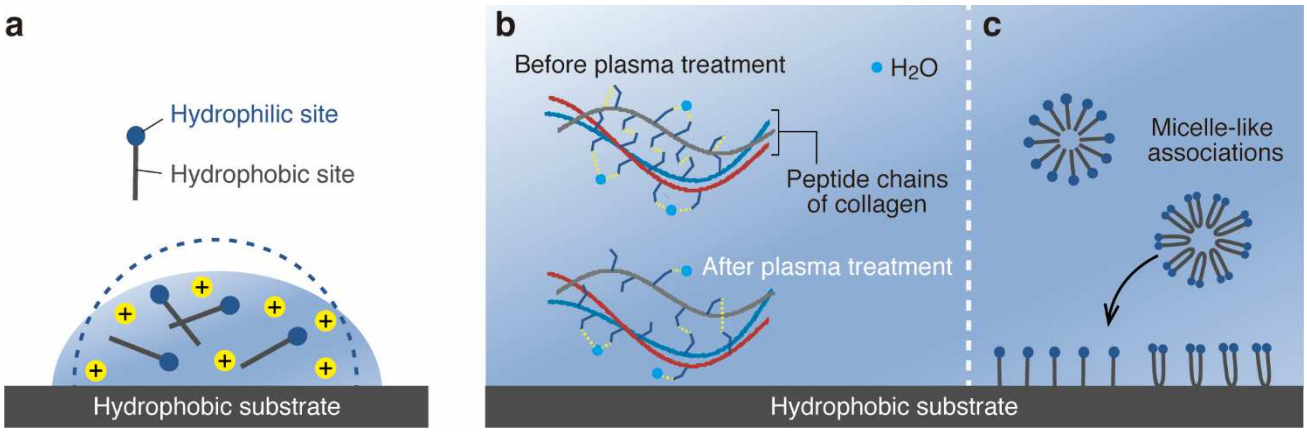

Supplementary Fig. 10. A possible mechanism by which plasma induces functionalization of collagen solution, leading to biofunctionalization of hydrophobic substrates. (a) Electric charge–driven changes in surface and interfacial properties of collagen solution, leading to an increase in wettability on hydrophobic surfaces. **(b)** Plasma causes changes in the local conformation and hydrogen bonding states of collagen molecules without inducing global changes in the structure of collagen molecules. **(c)** Plasma treatment induces the collagen molecules to assume a micelle-like association that leads to an increase in reactivity with hydrophobic substrates.

Description of Additional Supplementary Files

File Name: Supplementary Movie 1

Description: Time-dependent variation in a droplet of collagen solution (*left*) or plasma-treated collagen solution (*right*) on a hydrophobic cover glass. Movie shows 150-s change at a frame rate of 5 fps.

Supplementary Files

This is a list of supplementary files associated with this preprint. Click to download.

- SupplementaryMovie1.avi